CHERENKOV DETECTORS FOR TRANSMISSION STUDIES OF MONOENERGETIC HIGH-ENERGY PHOTONS IN ACTIVE INTERROGATION APPLICATIONS

A Thesis
Presented to
The Academic Faculty

by

Paul B Rose Jr

In Partial Fulfillment
of the Requirements for the Degree
Master of Science in the
School of Mechanical Engineering
Nuclear and Radiological Engineering Program

Georgia Institute of Technology
December 2015

CHERENKOV DETECTORS FOR TRANSMISSION STUDIES OF MONOENERGETIC HIGH-ENERGY PHOTONS IN ACTIVE INTERROGATION APPLICATIONS

Approved by:

Dr. Anna S Erickson, Advisor
School of Mechanical Engineering
Nuclear and Radiological Engineering Program
Georgia Institute of Technology

Professor Nolan Hertel
School of Mechanical Engineering
Nuclear and Radiological Engineering Program
Georgia Institute of Technology

Professor C.K. Chris Wang
School of Mechanical Engineering
Nuclear and Radiological Engineering Program
Georgia Institute of Technology

Date Approved: November 24, 2015

ACKNOWLEDGEMENTS

This material is based upon work supported by the National Science Foundation under Grant No. ECCS-1348366 and by the U.S. Department of Homeland Security under Grant Award Number 2014-DN-077-ARI079-02. The views and conclusions contained in this document are those of the authors and should not be interpreted as necessarily representing the official policies, either expressed or implied, of the U.S. Department of Homeland Security. This work is a part of the ARI collaboration with Massachusetts Institute of Technology (R. Lanza) and Pennsylvania State University (I. Jovanovic).

Special thanks to Peter Binns of MIT Bates Linear Accelerator Center for help with operating the accelerator and going the extra mile to make sure things run smoothly. You are an invaluable asset at the facility and a good friend.

Thanks to the Achievement Rewards for College Scientists (ARCS) foundation for recognition and financial support. Also, thanks to the Roy G Post Foundation for recognition and financial support.

TABLE OF CONTENTS

LIST OF TABLES

LIST OF FIGURES

SUMMARY

Active interrogation of cargo containers employing monoenergetic photons offers an expeditious low-dose approach in pursuit of shielded special nuclear materials. Cherenkov detectors can be used for a variety of purposes, including imaging of the cargo contingent upon gamma ray energies used in interrogation. If the gamma ray energies are sufficiently well separated, as the case in ^{11}B(d,n-γ)^{12}C reaction resulting in 4.4 MeV and 15.1 MeV photons, spectral analysis using Cherenkov detectors is possible. Applying an array of custom designed Cherenkov detectors reduce undesired low energy background, both natural and scatter from the application environment, while producing the capability of high contrast transmission imaging. Spectral analysis of the image can be used to confirm the presence of high-Z materials by analyzing the relative transmission of the two main energies emitted by exploiting the large difference in Compton Scatter and pair production cross sections. These detectors require a special approach to design and energy calibration due to the lack of resolution in order for spectral analysis to take place. This thesis addresses the design and utility of Cherenkov detectors for active interrogation with monoenergetic photons as well as the results of computational and experimental studies of their energy calibration and application to imaging with material identification.

CHAPTER I

INTRODUCTION

Cargo examination using radiation methods is an integral part of US safety and security strategy [18], especially when searching for illicit small volumes, on the order of 100 cm^3, of special nuclear material (SNM) while in transportation. Development of a number of radiation-based scanning techniques, both passive [21] using the radiation signatures specific to materials of interest and active [10, 9, 17] with a radiation source employed, have been driven by the impracticality of physically opening and inspecting each incoming container from air, sea, and ground. Passive techniques stand out with low cost and relative simplicity as compared to active interrogation systems, but solely rely on radiation naturally emitted from SNM, which is easy to conceal with various materials as shielding [7]. Active interrogation methods usually suffer from large doses delivered to the cargo, system operators, and potential stowaways. This dose is the result of techniques such as bremsstrahlung, continuous energy spectrum with a large low energy concentration, and neutron interrogation which impart a lot of unnecessary dose. However, an active interrogation system producing monoenergetic photons, generated as products of low-energy nuclear reactions, for example $^{11}B(d,n\text{-}\gamma)^{12}C$ [3, 14, 4, 12], can be applied to probe the shielding and reveal the SNM without delivering dose that is associated with bremsstrahlung-based systems. This significant reduction in dose delivered to the cargo and surroundings leads to a desirable active interrogation source. Coupling high energy monoenergetic photons to an array of specifically designed detectors leads to the capability of studying gamma ray transmission through the cargo and production of a high contrast planar image. Such a detector-source combination also takes advantage of properties specific to nuclear

materials, such as delayed neutron and gamma emissions, to add more dimension to the system. A conceptual illustration of a proposed transmission imaging using an array of Cherenkov detectors is shown in Figure 1.

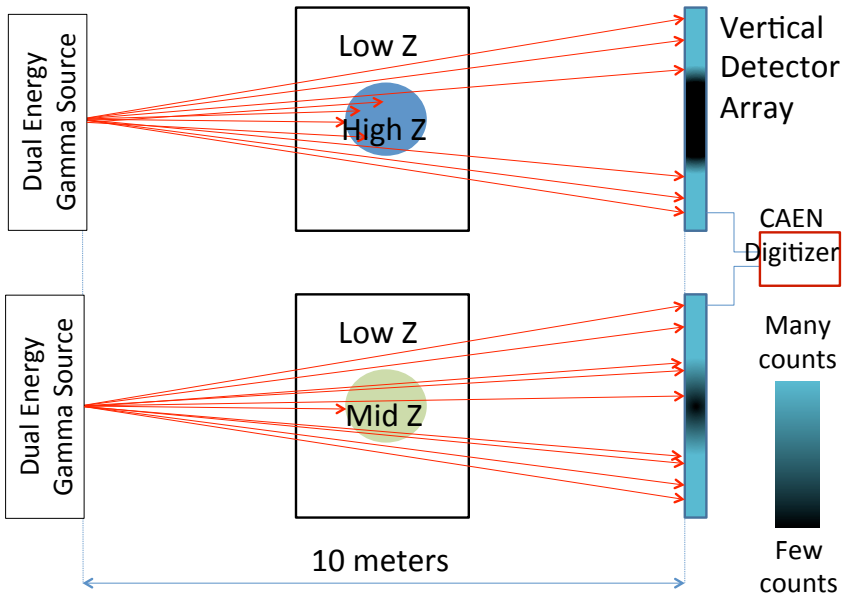

Figure 1: Conceptual design and principle of operation of imaging system based on monoenergetic photons.

This thesis addresses the results of computational and experimental studies leading up to a proof of concept system including energy calibration [16] performed with Cherenkov detectors designed [15] specifically for an active interrogation system designed for gamma ray transmission imaging. Also discussed is spectral unfolding of the transmitted radiation detected to produced a measure of the atomic number, Z, of the material for a rapid identification of heavy items in a cargo container.

CHAPTER II

SYSTEM OVERVIEW

2.1 Source of monoenergetic photons

Multiple methods are available for producing high energy photons for active interrogation purposes such as bremstrahlung, inverse Compton scatter, and nuclear reactions. While all have their merits, nuclear reactions with multiple well separated high energy gamma rays seem to have the most promise for Cherenkov applications. Many low-energy nuclear reactions can produce high energy gamma rays [3], but for the purposes of this thesis the focus on an extension of one system in particular [13, 12]. In this system, a compact accelerator is employed to impact deuterons into a ^{11}B target, mainly resulting in a ^{11}B(d,n-γ)^{12}C reaction. The reaction is driven by a modified LANSAR Model DL-3 radiofrequency quadrupole accelerator manufactured by Accsys Technology Inc. and located at the Massachusetts Institute of Technology Bates Linear Accelerator Center (Middleton, Massachusetts). The accelerator produces a 3-MeV d^+ beam with versatile pulse rates and widths, delivering an average current of up to 90 μA at up to 800 Hz repetition rate with a duty cycle of up to 1.6% according to the factory acceptance test [8].

The target design used for systems such as this are complex due to the heat generated from the impinging deuterons. The mounting and thickness of the target need special attention to balance heat removal and deuteron interaction probability. Thin targets mounted to a metal backing are effective at mitigating the low thermal conductivity of boron but may not stop the deuteron causing reaction with the metal so the target thickness must exceed the range of the deuteron. Most systems using this reaction employ a high purity, enriched boron target, usually 99.9% ^{11}B to focus

Table 1: DL-3 Operating Specifications.

Parameter Description	Measured Value
Output d^+ beam energy	3.02 MeV
Beam pulse width	2 - 150 μsec
Beam repetition rate	80 - 800 Hz
Max RF duty factor	1.6%
Output beam current pulsed	$6 - 10\,\mathrm{mA}$
Beam diameter at target entrance	$10\,\mathrm{mm}$
Vacuum pressure	$3 \times 10^{-7}\,\mathrm{torr}$
Average current	$1 - 90\,\mu\mathrm{A}$
RF fill time	$5 - 6\,\mu\mathrm{s}$

on most desired photon energies. This experimental set up originally used a thick target of enriched boron, but the intense deuteron beam melted a hole in it before my experiments began. For my studies, a natural boron target was used with an approximate ^{10}B isotopic abundance of 19.9% and ^{11}B isotopic abundance of 80.1%. The thickness of the natural boron target was 2.0 mm and measured 25 mm by 25 mm. This target was purchased from Goodfellow USA, part number 433911/2. The boron was fastened to a high vacuum aluminum end cap using a custom machined steel flange as shown in Figure 2.

The incident deuteron leaves ^{12}C in excited states which produce intense 4.4 MeV and 15.1 MeV gamma rays as well as less intense gamma rays during carbon's return to the ground state. By time gating the data acquisition with the accelerator pulse, it is possible to filter out undesired products from nuclear reactions caused by the emission of high energy neutrons and focuses on the fastest de-excitations of the carbon nucleus. Experimental results validating this method can be found in Figure 3, taken from Sheffield and Taducci [20].

The 4.4 MeV and 15.1 MeV gamma rays are used to produce a transmission image of the cargo, identifying relative Z of the material. The 4.4 MeV photon interactions are heavily dominated by Compton scattering and therefore are a measure of the

Figure 2: Assembled natural boron target before installation.

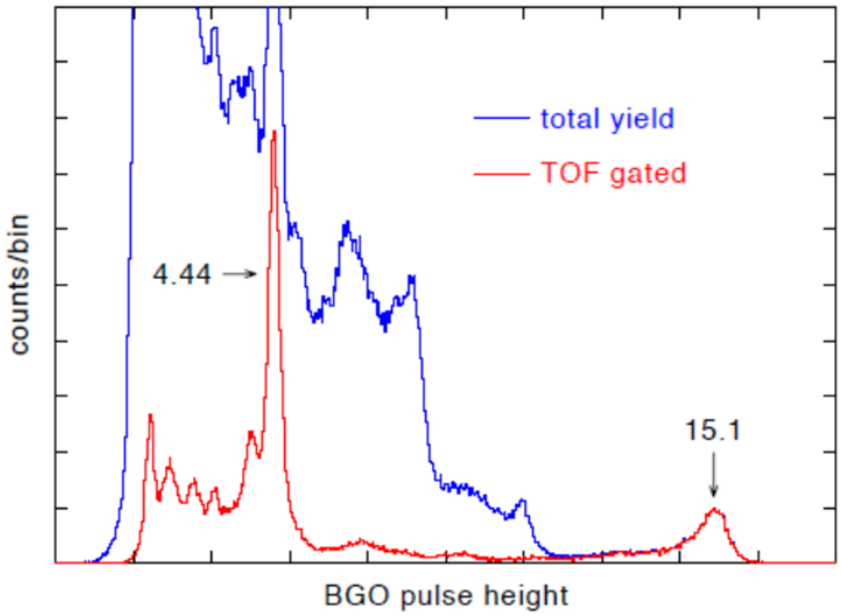

Figure 3: Time of flight gated energy spectrum. Adopted from Sheffield and Taducci [20].

electron density of the material which is a function of the Z. The 15.1 MeV interactions are dominated by pair-production for mid- and high-Z materials.

The work of Sheffield and Taducci [20] focuses on an enriched ^{11}B target while

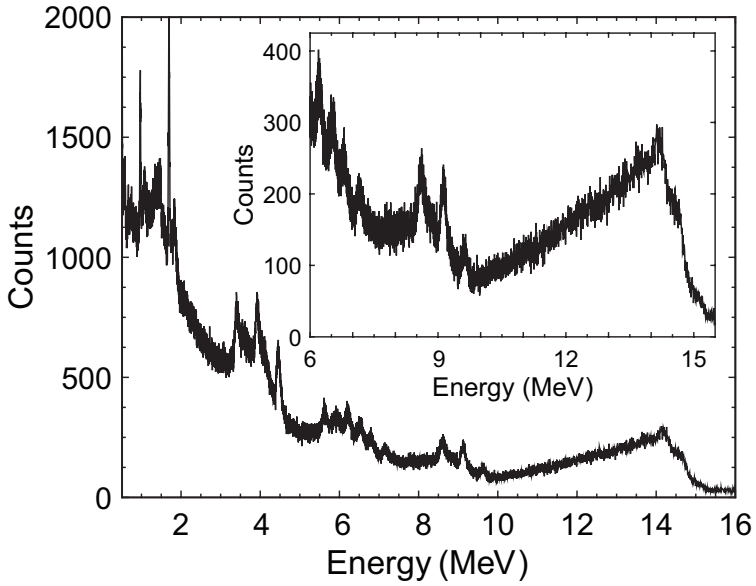

Figure 4: Energy spectrum of the source taken with LaBr detector.

most of the results for this project use a natural boron target. Slight variation is expected from their results due to the target being only 80.1% ^{11}B, but the most prominent reactions should be consistent. Figure 4 shows a measurement of the source used in this project by a 1.5 inch diameter LaBr detector from Canberra. This was done without time of flight gating or collimation as in the previous work. The measurements made by Sheffield and Taducci were done with a 3 inch BGO detector which has a very high density and they collimated the beam so it only hit the center of the detector which maximized full energy deposition. The LaBr crystal is still high density, but not as dense as the BGO. However, this measurement confirms an abundance of 4.4 and 15.1 MeV gamma rays from the source.

2.2 Shielding and collimation

The source is housed in an non-shielded warehouse adjacent to a parking lot. The radiation safety officer on site mandates the combined neutron gamma dose rate outside the walls of the warehouse be kept below 0.5 mrem h^{-1} which limits the operating current of the accelerator. To increase the beam current as much as possible while

also observing the principle of ALARA, the target itself is heavily shielded in all directions except the direction of the detectors. The ^{11}B target is surrounded by a cave of lead, then borated polyethylene is stacked on all sides to reduce the radiation being emitted over 4π from the nuclear reaction.

The neutrons from the ^{11}B(d,nγ)^{12}C reaction were filtered out of the beam line using a 14-inch thick block of borated polyethylene placed between the source and the interrogated object. The neutron filter does a good job of filtering out neutrons while allowing the high energy gammas to pass through relatively unimpeded. Some of the low energy products, such as the typical 511 keV annihilation photon, are significantly reduced which helps to minimize dose to the cargo. The radiation produced is collimated using a combination of lead, borated polyethylene, and two rows of large concrete blocks separated to produce a cargo lane before the imaging detector array as shown in Figure 5. These multiple layers of collimation result in fan beam spanning the height of a cargo container.

Figure 5: Boron target surrounded by lead and borated polyethylene, then collimated using large concrete blocks.

The concrete blocks included a small gap, 2.5 cm in the first set and 5 cm in the second, to create the fan beam. The area between the two rows of concrete collimators is used as the interrogation area, therefore collimating the radiation exiting the material before the detector array.

2.3 Imaging detector array

The full imaging array will cover the height of a cargo container and contain two columns of detectors that are offset vertically to maximize image resolution while minimizing the footprint of the array. This will require 192 detectors, 96 in each row to cover the full 2.44 m height of a typical cargo container.

The experiments conducted as part of this work used a mini array of 8 prototype detectors. Time and funding restrictions prohibited the construction of a full size array. The full size array is not necessary for completion of this work as this is supposed to show a proof of concept system, not a finalized commercial product.

2.4 Electronics and readout

The signal from all 8 detectors was analyzed by a single 8 channel desktop digitizer from CAEN. This DT-5730B uses a digital pulse processing - pulse shape discrimination (DPP-PSD) firmware to integrate the charge from the pulses to create a histogram. The hardware is coupled to CAEN's DPP-PSD control software for easy readout and stored for analysis. This digitizer includes a large amount of on-board memory to store new events for processing in the event of high count rates. This feature virtually eliminates dead time from electronics vastly improving the array performance in such a demanding atmosphere.

CHAPTER III

DESIGN AND OPTIMIZATION OF CHERENKOV DETECTORS

3.1 Cherenkov radiation and its applications

Cherenkov light emission [5, 6] is a response of matter to the motion of a charged particle traveling at a speed exceeding the phase velocity of light in that medium. Slow moving charged particles create symmetrical polarization in a medium and thus do not create an electric field. Particles exceeding the phase velocity of light result in polarization along the axis of motion creating a dipole field. When this field collapses, an electromagnetic pulse (Cherenkov radiation) is emitted in the forward direction, similar to a sonic boom from a super sonic jet. It is commonly produced in dielectric materials through Compton electrons or pair-production electrons and positrons. The intensity of light produced by this process is much less than that of luminescence (the basis for scintillation detector operation) requiring more sensitive optical photon detection equipment such as low light photo-multiplier tubes (PMT). The amount of optical photons produced is related to the energy of the charged particle. Energy transferred from a photon in a Compton (Klein-Nishina formula) or pair production event is continuous therefore Cherenkov light production is also continuous. This leads to challenges around detector design and spectral analysis as discussed in subsequent sections. On a positive side, typical scintillator detectors have a decay time measured in microseconds while Cherenkov radiation is nearly instantaneous and with fast pulse processing equipment can be measured in picoseconds. Other unique properties distinguishing Cherenkov radiation from luminescence are a UV-concentrated photon spectrum and inherent energy threshold that is related to the

dielectric constant of the chosen material.

Cherenkov radiation is emitted in a forward cone in the direction of the charged particle which is also forward peaked for maximum energy transfer Compton events. At higher incident gamma ray energies pair production becomes the dominant reaction which is also forward peaked. This cone is emitted in the direction of the PMT or other photon sensing device making detector design crucial for peak results. The inherent energy threshold properties of Cherenkov radiation are based on the refractive index, n, of a material which sets the phase velocity of the speed of light, c, in that material which the velocity of the charged particle must exceed as shown in Equation 1.

$$v > \frac{c}{n} \tag{1}$$

The refractive indices of materials can be finely tuned to produce an energy threshold rejecting particles below a certain energy suppressing natural background radiation as well as undesired signal from many activation products. Significant background reduction focuses resources on the energies desired thus further reducing the demands on the detector allowing for faster scanning times. Figure 6 illustrates the relationship of the Cherenkov threshold to the energy of the incident gamma rays and subsequent Compton electrons.

This is referred to here at the absolute threshold as only electrons/positrons with this minimum kinetic energy can product Cherenkov radiation. The light generation is very low for particles near the threshold as shown in Figure 7 and is often lost in optical efficiency or in PMT noise. For practical purposes we need to define effective threshold which is when the photon consistently transfers enough kinetic energy to the charged particles to overcome these challenges. This will be discussed more in the detector design section.

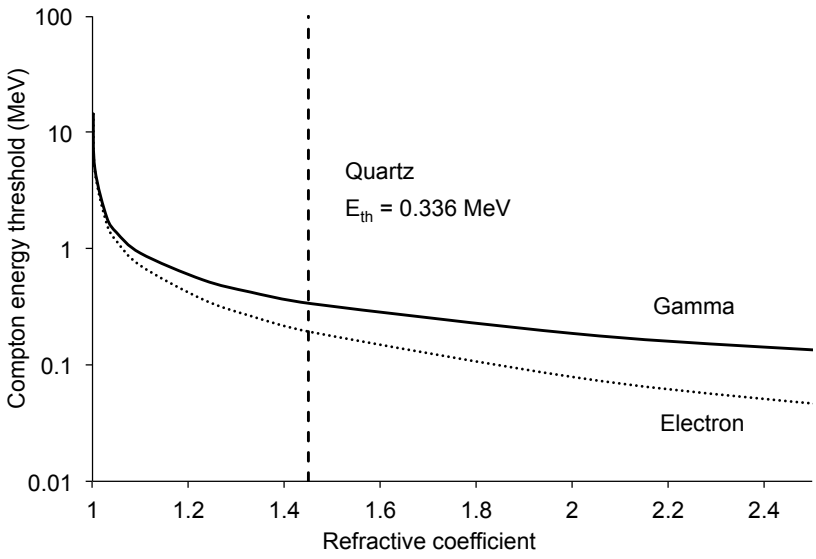

Figure 6: Natural threshold of Cherenkov radiation as a function of refractive index.

3.2 Modeling of the detector with GEANT4

Performance of the detectors has been characterized and optimized using Monte Carlo simulations. Geant4.10 was used to model the detectors due mainly to the capability of advanced optical photon transport and validated Cherenkov physics. Geant4 also allows the user precise control of material properties, atomic and optical as a function of wavelength, as well as surface properties to properly handle material boundaries which is lacking in MCNP. The Geant4 toolkit [1, 2] provides a flexible framework for the simulation of particle transport and interaction with matter.

The accuracy of the simulations relies heavily on user defined parameters for detailed properties and physical processes of interest. Geant4 has the capability of triggering and tracking optical processes, which includes the generation and propagation of Cherenkov photons by a charged particle. Rayleigh scattering, bulk absorption and reflection-refraction media-boundary interactions are also part of the optical processes and are wavelength-dependent. Mechanical and optical properties of quartz from experimental measurements were combined with information provided by the

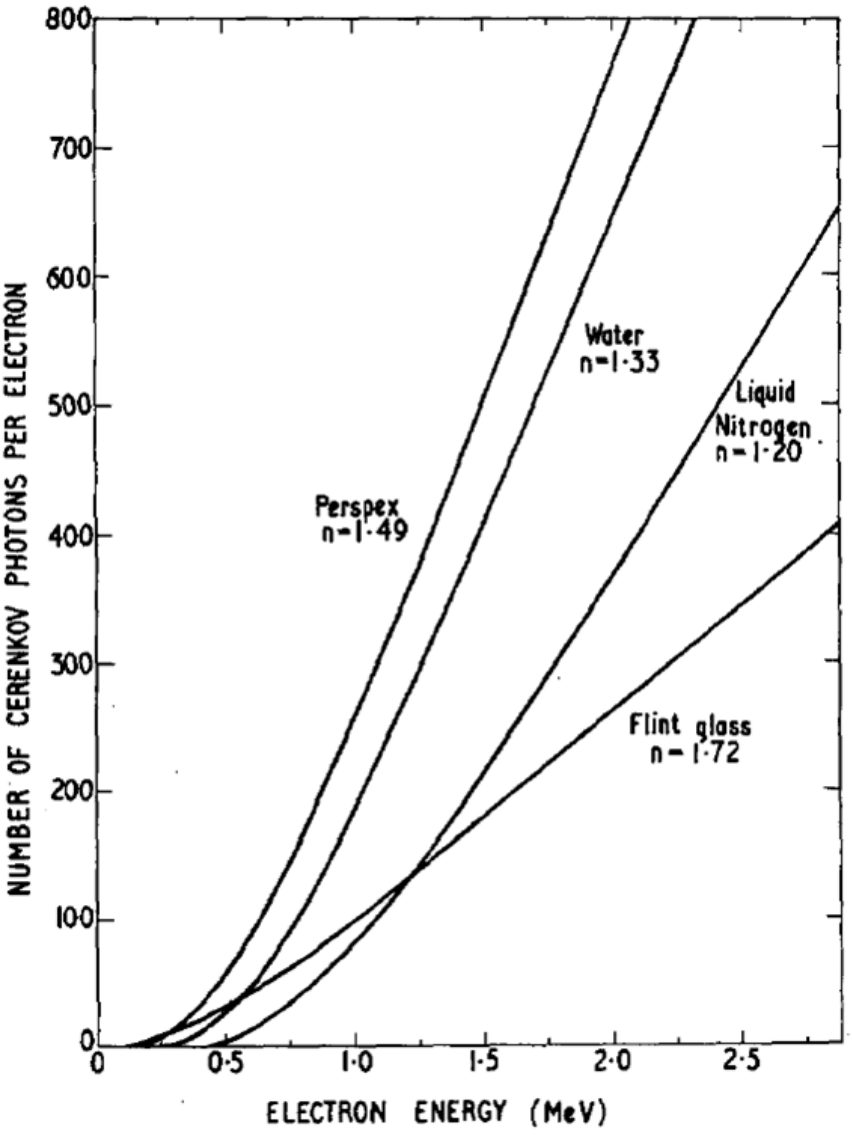

Figure 7: Photon yield as a function of electron energy as taken from Sowerby [19].

manufactures including the efficiency and sensitivity of photomultiplier tubes. Including the PMTs wavelength-dependent quantum efficiency in the simulation yields a method of testing configurations before buying expensive equipment. Modeling studies included the quartz crystal size and shape combined with a variety of PMTs to determine the optimal configuration for the given application.

Prior to detector construction, the efficiency of the assembled components has been studied as a function of γ-ray energy and the PMT properties assuming 100%

geometric efficiency. The sources included ^{137}Cs, ^{60}Co, ^{232}Th, PuBe, and AmBe, as available in the laboratory for experimental validation. AmBe and PuBe sources are of particular interest as a surrogate for the lower energy region of the deuteron-induced spectrum to be used in the final system. Both of these sources emit 4.4 MeV gamma rays from the same ^{12}C excited state transition as the accelerator driven source. Since the actual ^{11}B(d,n-γ)^{12}C reaction also produces prolific amounts of neutrons, hydrogenous materials were studied in order to understand the shielding needs of experimental accelerator-driven reactions. The neutrons were less of a concern When the main detector design was switched from PMMA to quartz but the neutron shielding material is still preferred to reduce other n-γ interactions in the experimental hall. AmBe and PuBe sources were combined with polyethylene (poly) cylinders producing neutron capture by hydrogen resulting in a 2.2 MeV gamma ray. Materials rich in hydrogen may be used to shield neutrons during the active interrogation. Depending on the material selected, some will create a significant contribution to the signal due to the capture reaction. By including the neutron in the simulation, improved accuracy of the lower end of the anticipated spectrum is obtained while also allowing for preliminary validation and transmission experiments to be carried out. The summary of the simulated efficiency for the sources is shown in Table 2. This metric is the theoretical maximum as it counts even single photo-electrons generated in the PMT. This is a slight overestimate as some of the signal will be filtered out as dark current in the PMT. This simulation indicates roughly 10% events imparting between the absolute threshold and effective thresholds result zero photo-electrons generated in the PMT.

The detector efficiency is dependent upon many things but primarily on the energy of the photon as well as the length of the detector. Most scintillating detectors have a higher efficiency with ^{137}Cs (662 keV γ-ray) than they do with higher energy sources which is not true for these Cherenkov detectors. The effective energy threshold for

Table 2: Detector intrinsic efficiency by source.

Source	Photon energy (keV)	2" long radiator	4" long radiator
^{137}Cs	662	19.6%	25.4%
^{60}Co	1173 and 1332	33.9%	51.5%
^{232}Th	2614 (maximum)	30.8%	49.1%
PuBe	4440 (maximum)	25.8%	45.8%

photon-generated signal of these detectors is about 550 keV, meaning the electron must receive a vast majority of the energy during the Compton scatter from the 662 keV photon. The scattering angle probability is not forward peaked at this energy and can result in many angles resulting in low energy transfer as predicted by the Klein-Nishina formula. This means that most Compton interactions will not impart enough energy to the electron to effectively generate Cherenkov radiation. The relationship between photoelectrons produced in the PMT and the incident particle energy can be deduced similarly to the energy calibration method introduced earlier. However, since the simulation is sequential, there is no pile-up or multi-particle coincidence to be observed. Therefore the highest number of photo-electrons produced corresponds to the maximum energy transfer to the charged particle. To ensure the simulation is kept consistent with experimental studies, a 0.2% cutoff for the energy calibration is employed here as well. Considering the physics behind the interactions, the total energy deposited is always less than the energy of the photon emitted by the source. However, since this is common across all photon interactions in the energy range considered, the relation between the photon energy can be established as shown in Figure 8.

The points on the plot represent the maximum γ-ray energies of the sources used from low to high: ^{137}Cs, ^{60}Co, ^{232}Th, and PuBe, respectively. The results are shown for the 2-inch long detector, and the 4-inch long design displays a nearly identical relationship. The simulation predicts a highly linear relation between the energy

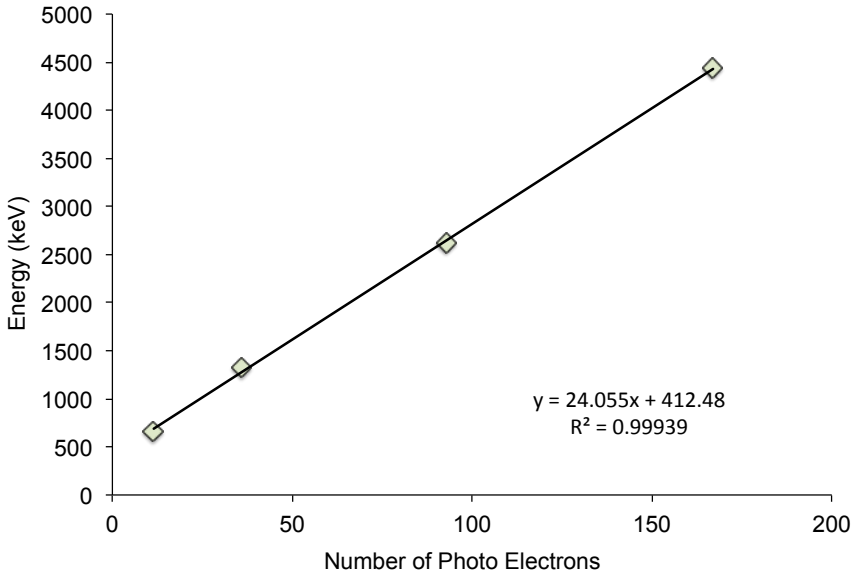

Figure 8: Simulated γ-ray energy calibration of the 2-inch long quartz detector.

deposited in the detector and the number of photoelectrons created in the PMT across this incident photon energy range. These relationships are used to produce the energy calibrated histograms for the detector fabricated for experimental testing as shown in Figure 9. The x-axis is the number of photo-electrons produced calibrated to incident photon energy in the R292 PMT, which has high UV sensitivity. This curve is not exactly what is expected experimentally because the photo-electrons have some energy distribution to them where the simulation assumes a constant energy. The simulation also does not consider gain in the PMT which is also nonlinear. It should be noted that additional studies were performed to include 15.1 MeV gamma rays. Due to the higher energy of the gamma ray, the interactions are a combination of Compton scattering and pair production which leads to deviation from linearity observed in Figure 8 and quadratic energy calibrations are needed. This result was neglected here because the accuracy of the lower energy sources are not evident with the spectrum extended to 15.1 MeV.

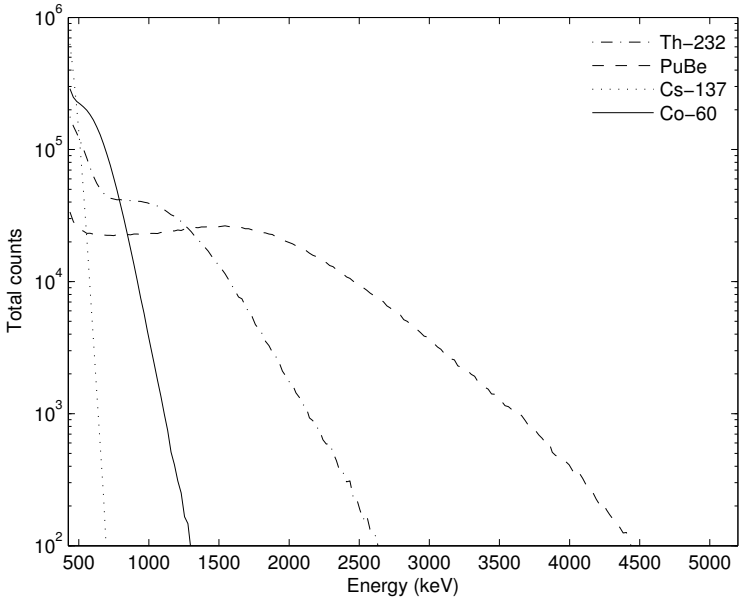

Figure 9: Calibrated spectral response of the 2-inch long detector (simulation).

3.3 Energy calibration technique

Energy calibration for scintillation and semi-conductor detectors is a well-understood process that uses either the maximum or centroid of a peak in the energy histogram to derive the incident particle energy versus energy bin relationship. These traditional methods do not work for Cherenkov radiation since there are no well resolved peaks due to the continuous nature of Cherenkov radiation and low levels of light emission for particles in MeV energy range. Instead, one must consider features in the energy histogram and relate them to the physics taking place. Using features such as the tail slopes, inflection points, intercepts, and shoulder we can assign an energy versus bin relationship. The intercept of the two slopes in the tail indicates the maximum energy deposition, signal higher than this point are pileup events or high energy cosmic background. Inflection points often correlate to the most probable Compton electron energy corresponding to the energy of incident photon. Shoulders in the spectra indicate the average energy deposited by a monoenergetic photon.

In the detector calibration approach developed as part of this thesis, the primary source of particle information is the "tail" of the energy histogram as shown in Figure 10. In an ideal scenario, the location of the tail with respect to the energy bin axis will indicate the energy calibration point of maximum energy transferred. However, very high flux situations produced by accelerators are far from ideal when considering spectral analysis. The Cherenkov detectors were designed to work in such environments; although statistically rare due to the fast nature of the electromagnetic emission taking place, pulse pile-up events occur affecting the spectrum tail. Thus, the intercept of the tail to the energy bin axis cannot be considered as the maximum energy transferred. When analyzing the tail of a Cherenkov spectrum resulting from such high flux environments, we look at the point of the tail where it appears as two linear relationships intersect as shown in Figure 10. Experimentally observing the pile-up effects in various high flux conditions, we choose to cut off everything below 0.2% of the total signal. The steeper slope of the spectrum tail is then extrapolated to this cutoff using a linear fit resulting in an intercept with the energy bin axis. This intercept is chosen as the maximum energy transfer from the photon to the electron.

This method can be employed using sources and inducing pileup if necessary. Consider the PuBe and AmBe detector responses, both emit a maximum photon energy of 4.438 MeV as a result of the Be(α,γ)C reaction. Both sources were used the same distance from the detector but the AmBe source is 50 times stronger than the PuBe source, hence the AmBe has a larger ratio of pulse pileup (signal above channel 7000) to the shoulder located at about channel 5000. The intersection of the AmBe and PuBe tails happens at the intersection of the two linear slopes from each spectra. This point also coincides with the 0.2% cutoff. Similar results can be achieved for other sources by using sources of varying intensity or simply changing the distance from the source to the detector taking advantage of the $1/R^2$ relationship

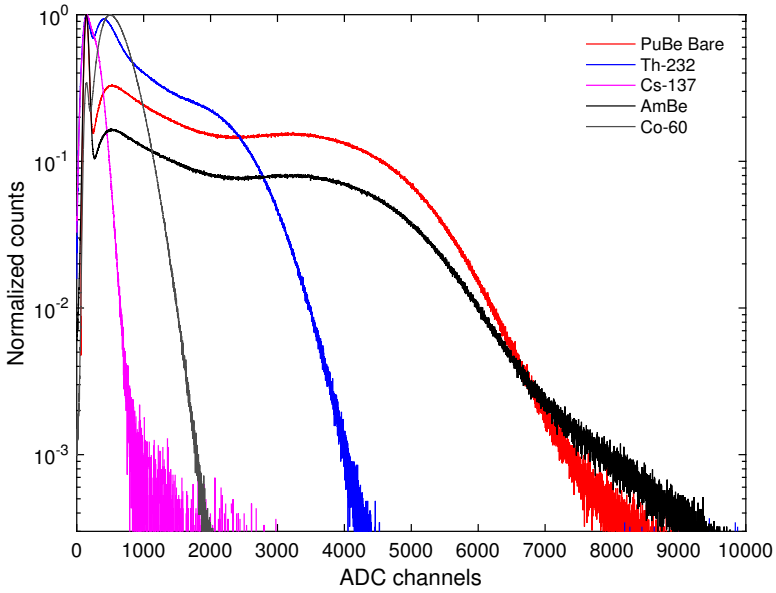

Figure 10: Cherenkov emission spectra associated with different sources. All data have been normalized to 1 to account for the differences in activity of these sources.

of the source.

This 0.2% metric is specific to the detector and electronics and will vary for different systems. However, using this cutoff metric, we can assign the location where the energy histogram intersects the new x-axis as the maximum energy deposited from the incident photon which provides the relationship for channel vs. incident particle energy needed for energy calibration. This relation will hold for most sources, unless very high fluxes are experienced as compared to the reference system. To be consistent in assigning this intercept, an algorithm was developed to analyze the slope of the remaining tail and solve for the ADC channel where the linear relationship meets the new cutoff. This algorithm must be tailored to each detector as it takes into account the slopes of the tail to indicate event pile-up.

3.4 Detector design

High radiation flux active interrogation systems pose intricate detection challenges which Cherenkov detectors are well suited for. High energy resolution is not a priority

in such a system since the 4.4 MeV and 15.1 MeV gamma rays are well separated. In order to have a viable imaging system the detectors must be scalable, customizable, constructed from inexpensive materials, resistant to undesired radiation, and capable of processing high interaction rates.

The initial prototype detectors were constructed from Polymethyl methacrylate (PMMA) from Eljen Technology. Two types were purchased for testing, an ultraviolet absorbing (UVA) $2.54 \times 2.54 \times 30\,\text{cm}$ bar and an ultraviolet transmitting (UVT) 2.54 cm diameter rod 30 cm in length. The chemical compositions were nearly identical, $C_4H_6O_2$, bu there was a proprietary additive to the UVT rod to increase the photon internal transmission. The density of this material is $1.14\,\text{g}\,\text{cm}^{-3}$ and an index of refraction of 1.5. Such a low density is not ideal for photon detection, especially at 15.1 MeV, so the length of 30 cm is crucial to boost detection efficiency. If purchasing enough material for a large array, Eljen quoted a price of $40.20 per rod with optical grade polishing.

The reflector chosen for construction of the detector was dictated mainly by cost vs benefit. There are some highly efficient reflectors that could be used such as GORE DRP. This is a diffuse reflector made of expanded PTFE with proprietary processing in sheets as thin as 1 mm. Samples were purchased and evaluated but showed no discernible difference in testing against Teflon PTFE tape also known as pipe thread sealant. This tape is very inexpensive and is made from the same material as GORE DRP with slightly different processing. The GORE DRP does not bend well or adhere tightly to the Cherenkov radiating material, especially the bar with sharp edges. The thinner 0.7 mm tape can be wrapped very tight around the radiator for increased reflection efficiency. The tape was sourced from McMaster-Carr, part number 4591K14 and costs only $3.95 per roll of 14.6 m. This gives enough coverage for 5 layers thick on 4 detectors.

Light-proofing was achieved by using black vinyl tape. This is standard grade

electrical tape sourced from McMaster-Carr part number 7619A11 at a cost of $0.95 per 18 m roll. Two layers were wrapped in an overlapping fashion to ensure integrity from ambient light.

These assembled materials were married to a Hamamatsu R6095-03 29.5 mm diameter, Bialkali Photocathode, 11-stage PMT using Saint Gobain BC-630 optical coupling grease. These PMTs and optical grease both have a lower operational limit of 300 nm which cuts off a large portion of the UV dominant Cherenkov spectrum. This was far from ideal, but the PMTs were available at no cost as they were disassembled from an array no longer in use to save on costs. The main benefit of these PMTs is a rise time of 4 ns taking advantage of the ultra fast Cherenkov process. These detectors were able to process an event every 6 ns.

The initial prototype detectors produced energy resolution worse than originally anticipated. They worked under the harsh environment testing, as presented later in this thesis, but were not desirable for the final system as some energy resolution is needed. Upon testing, two main issues were found; the photon absorption length originally provided by the company were incorrect, and the detectors suffered from H(n,γ)D capture reactions producing 2.2 MeV γ-rays inside the detectors.

Since there are neutrons present in the ^{11}B(d,n-γ)^{12}C reaction, a new Cherenkov radiator was chosen to be resistant to neutron neutron reactions such as the H(n,γ)D capture reaction. These secondary reactions can add massive overhead to the system and degrading the dual monoenergetic benefits of the available nuclear reaction. After considering and testing many other materials, Quartz, GE type 214 was selected as a final radiator option due to a very pure SiO_2 crystalline lattice structure with excellent light transmission properties, especially in the UV part of the spectrum.

Quartz provides a unique set of material properties well suited to this application. At 2.2 g cm^{-3} it has a higher density than most other materials typically used for

Cherenkov radiation allowing to use smaller detectors to match the photon interaction probability of the PMMA. An index of refraction of 1.46 gives a slightly higher threshold than PMMA which is beneficial for cutting off more low energy signal, thus further reducing overhead on the system. Quartz is not hydrophilic like many scintillator crystals and is very resistant to thermal expansion in the anticipated outdoor operating temperature range, -10 to 40 °C. The internal light transmission is efficient due to high purity of material and high internal reflectivity, allowing more optical photons to reach the PMT. Prototypes were first constructed of samples provided by Technical Glass Products, Inc of 5 cm and 10 cm in length. The geometry chosen for production is rods 2.5 cm in diameter by 15.2 cm in length. The quartz radiator is wrapped with the same PTFE tape reflector mentioned earlier, then light proofed with a rubber heatshrink. This combination has proved to be a very efficient, rugged design that is very resistant to neutron activation and can be used in the field under any weather conditions. An example of this combination can been seen in Figure 11 during construction of one the detectors.

Three quartz detectors combinations were constructed and used in testing: (1) a single 2.5 cm long quartz crystal coupled to a Hamamatsu R292 photomultiplier tube (PMT) with quartz window and sensitivity limit of 190 nm; (2) a single 5 cm long cylindrical quartz crystal coupled to a Hamamatsu R6095-03 PMT with a sensitivity limit of 300 nm; and (3) an array of six 15 cm long quartz crystals coupled to Hamamatsu R374 PMTs with UV transmitting glass windows and a sensitivity limit of 185 nm. The windows of the R292 and R374 PMTs are also made of quartz, reducing the light loss on the boundary. To take advantage of the additional wavelength range the optical grease used was made by Rexon, part number RX-600K. This is more expensive than the previous grease, however taking advantage of the additional light collection yields better performance. During analysis, the detector configuration was taken into account in order to compare the signal among different designs.

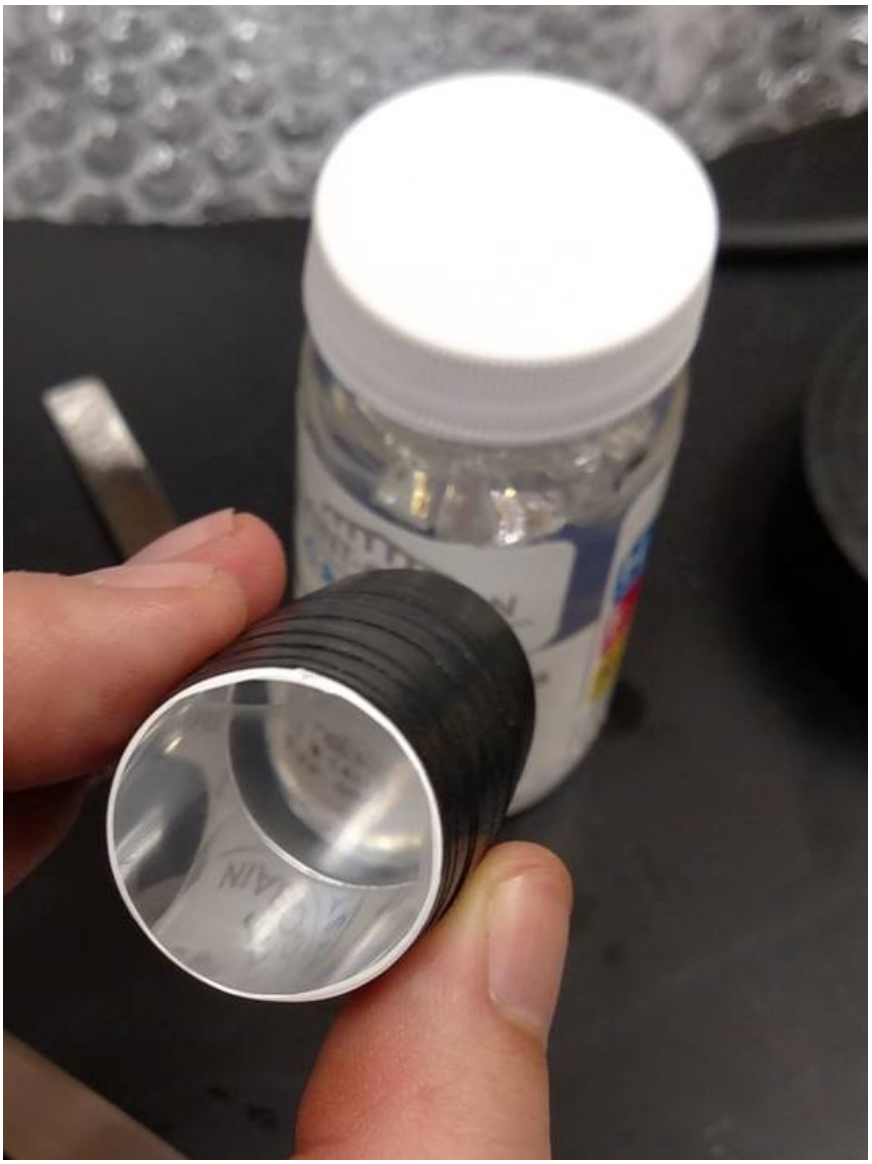

Figure 11: Construction of 2.54 cm diameter quartz detector.

The absolute Cherenkov energy threshold for this type of quartz, SiO_2, is calculated to be 0.336 MeV. This threshold is calculated assuming maximum energy transfer in a Compton scattering event which is rarely the case, especially at lower energies. Optical photon generation will be very low until approximately 0.55 MeV, known as effective threshold, where the partial energy transfer consistently imparts enough kinetic energy to the Compton electron to generate Cherenkov radiation. A large portion of background radiation is below this threshold and therefore will not

produce any signal in the detector.

3.5 Experimental testing of detector designs

Multiple detector designs have been built and tested using the various materials under consideration to understand detector properties as a function of γ-ray energy and detector length as well as for computational model validation. An array of PMMA prototype detectors is shown in Figure 12. This configuration was used to test detector capabilities in the harsh environment of the Varian Clinac dual 6 and 18 MV bremstrahlung beam.

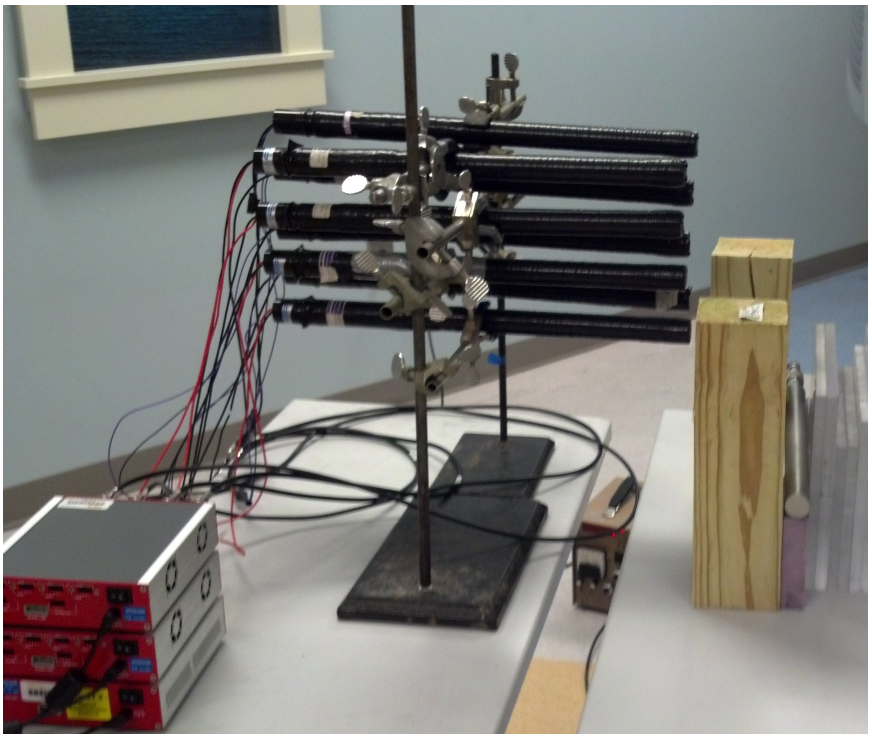

Figure 12: Experimental setup of various Cherenkov detectors for harsh environment testing in the 18 MV bremsstrahlung CLINAC beam at Georgia Tech.

The final validation was done with two quartz detectors of slightly different designs: a 2-inch long crystal coupled with a Hamamatsu R292 PMT and a 4-inch long crystal coupled with a R6095 PMT as previously described. Experimental energy calibration is more convoluted than computational due to the additional processes

neglected in the somewhat idealistic model. Statistically, event pile-up and multiplicity may be present even though Cherenkov radiation is a nearly instantaneous response to the charged particle; however, the effects are minimized when compared to scintillators or semiconductors. As described in the calibration method section, the first step is to apply a cut to the normalized counts to subtract the contribution of noise. The example of 0.2% of the total signal given then was calculated for this analysis. This also cuts off the signal from addition of two gamma rays as well as muon interactions which are much less probable than the photon interaction as observed in background measurements. Even though the size of the detector is small, an occasional muon interaction deposits a large amount of energy in the detector and can cause excess signal in any energy bin. Next, the slopes of the tails are analyzed and extrapolated to the location where they meet the x-axis (ADC channels) which then is correlated to the channel of full energy deposition (photopeak). These intersections are related to the maximum gamma energy emitted from the source. Figure 13 shows the resulting energy calibration relation for the 2-inch long detector. Even when results are pedestal-subtracted, the nonlinearity of Cherenkov light generation near the threshold region precludes low-energy photons from being used in any calibration. Photon resulting from ^{22}Na of 511 keV can cause signal in these detectors but even at full energy transfer they would fall into the non linear region between the absolute and effective thresholds. Photon energy of 661.7 keV corresponding to ^{137}Cs is the lowest energy used because it is just not practical to go any lower. When operating with the 15.1 MeV photon the ^{137}Cs point will be eliminated from the calibration as it won't be relevant to the energy range of interest.

Similarly to the computational results, the experiments show a strong linear relationship between energy deposited in the detector and the ADC channel. This trend line equation is used to convert the experimental data from ADC channels to energy of incident photons. The 4-inch long detector produced a very similar relationship

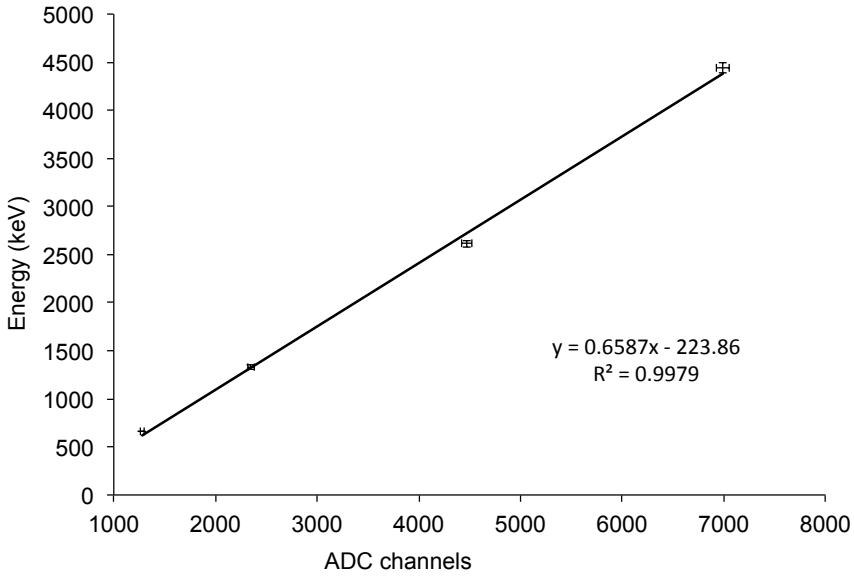

Figure 13: Experimental energy calibration of the 2-inch long detector.

and equation for the energy calibration. The resulting energy calibration can be seen in Figure 14 for the 2-inch long detector.

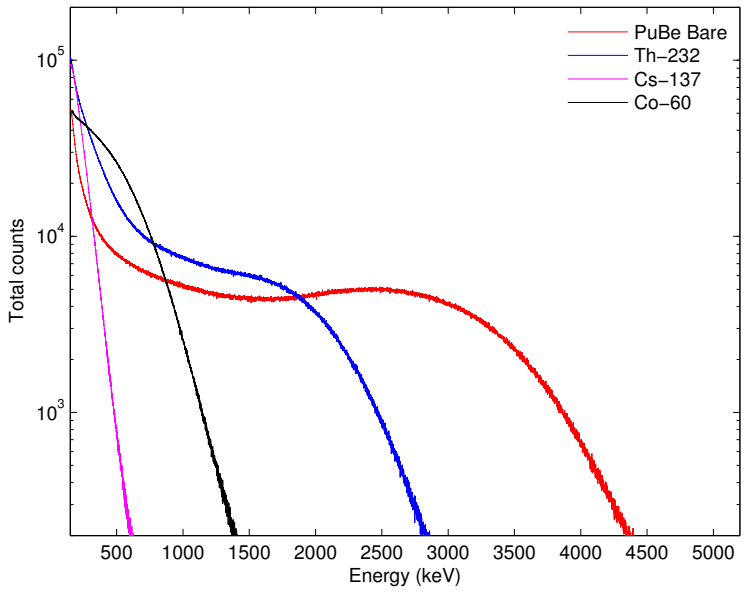

Figure 14: Calibrated spectral response of the 2-inch long detector (experimental).

When considering the Cherenkov spectra such as this, it is evident that there are no well-resolved peaks. Instead, spectral information must be obtained from slopes of

the tails and location of changes in slope, and shoulders. In the lower energy range, there is little usable data and Cherenkov detectors are only useful in Geiger mode or for timing. The peaks and shoulders that are most evident are related to the average energy transferred to the charged particles. The average energy transferred to a Compton electron in a 4.4 MeV scattering event from the PuBe/AmBe source is about 2.7 MeV. This is where the "peak" can be seen in Figure 14 in the PuBe spectrum. It is important to note the effective Cherenkov radiation energy threshold for a photon in this material is about 550 keV, and the linearity of the energy calibration breaks down in this region. If just the three higher energy sources (^{60}Co, ^{232}Th, and PuBe) are used a more accurate calibration is generated among those energies, but the 662 keV from the ^{137}Cs virtually disappears from the plot. For later experiments including 15.1 MeV photons, the 662 keV will be omitted from the energy calibration.

The 4-inch long detector uses the R6095 PMT which operates on a very different concept than the traditional box-and-grid style R292 used in the 2-inch long detector. The R292 is more efficient when considering total photo-electrons created vs. photo-electron collected, but the electron transit time is much longer, and the pulses are stretched over a longer time period due to the increased distance they must travel between PMT stages. This effect is on the order of 100 ns per pulse for the R292, where the pulse from the R6095 can be accepted in about 10 ns depending upon pulse analysis method. Figure 15 shows the same experiments performed with the 4-inch long detector with the energy calibration performed by the same method.

The energy calibration for the 4-inch long detector appears to be more accurate than the 2-inch long detector. Another characteristic to notice is the formation of peaks in the region less than 1 MeV. These peaks are misleading because they are formed due to the less efficient photo-electron collection method of R6095 PMT type. When few photo-electrons are generated as is usually the case in Cherenkov radiation, a large percentage could be lost at each stage. The more photo-electrons generated in

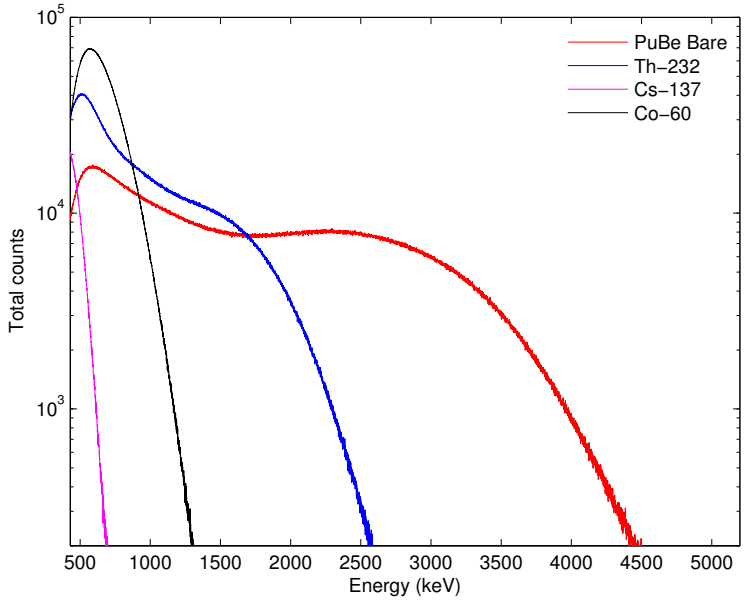

Figure 15: Energy calibrated experimental data from the 4-inch long detector.

the first stages, the more consistent the signal is. These faux peaks won't be visible in the presence of a scintillator attached to the same PMT. Even though the 4-inch long detector is twice as long, it registers fewer counts for the 662 keV photons than the 2-inch long detector did at the same distance from the source. The ratio of the maximum efficiency to the ^{137}Cs efficiency for each detector is much lower for the 4-inch long design due to the PMT type. The optical photon absorption and efficiency also plays a roll as the probability of the photon interacting in the first half of the detector is much higher than that of the second half. However, it is possible to see the difference in the "peak" between the combined peak from ^{60}Co (1.17 and 1.33 MeV γ-rays) and ^{232}Th (0.911 and 0.969 MeV γ-rays).

The PuBe and AmBe sources were used with and without hydrogenous material present surrounding the sources except for the direct line to the detectors. This produces a significant number of 2.2 MeV gamma rays from the (n,γ) reaction on hydrogen without altering the 4.4 MeV gamma emissions. Figure 16 shows the experimental results of detection of gamma rays from an AmBe source with and without

large poly cylinders around the source.

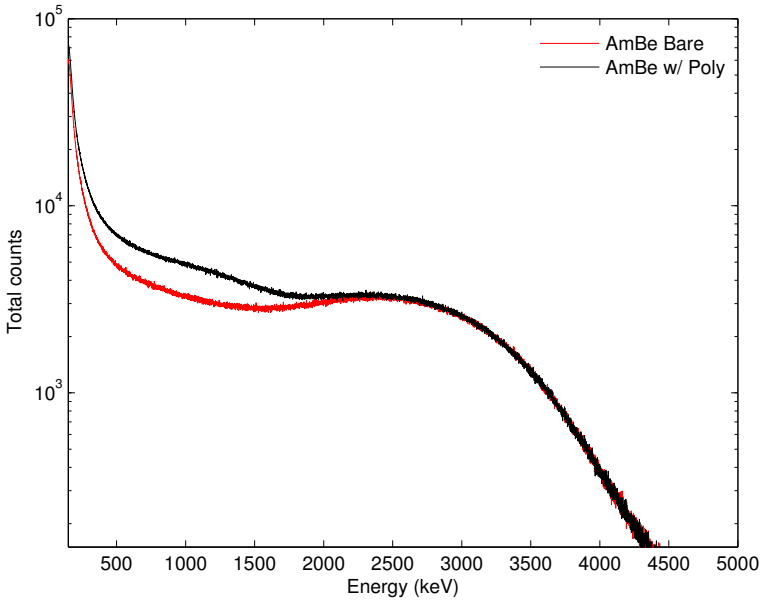

Figure 16: Comparison of moderated and unmoderated experimental results from AmBe source.

At the maximum γ-ray energy of 4.4 MeV, the two spectra line up very well as expected. The relative contribution of the 2.2 MeV gamma rays is very prominent in the run with polyethylene present. This mimics the low end of the accelerator driven source fairly well. The average energy transferred to a Compton electron in a 2.2 MeV scattering event is about 1.3 MeV which is where the shoulder can be seen in the spectrum where the poly is present.

Figure 17 illustrates the technique of Cherenkov detector energy calibration for both computation and experimental for comparison. The terminal energy (ADC bin or computational number of photo-electrons) of the peak is estimated. The estimate is then plotted against the corresponding energy of the incident particle. The slope of the line can be used to calculate the linear calibration parameters assuming the operation in the energy range of 4.4 MeV and lower. Besides the convenience of this method, using the terminal energy guarantees that when the detection threshold is

placed, it will not be exceeded by a particle of lesser energy. As is evident from the comparison, computational and experimental results are in good agreement.

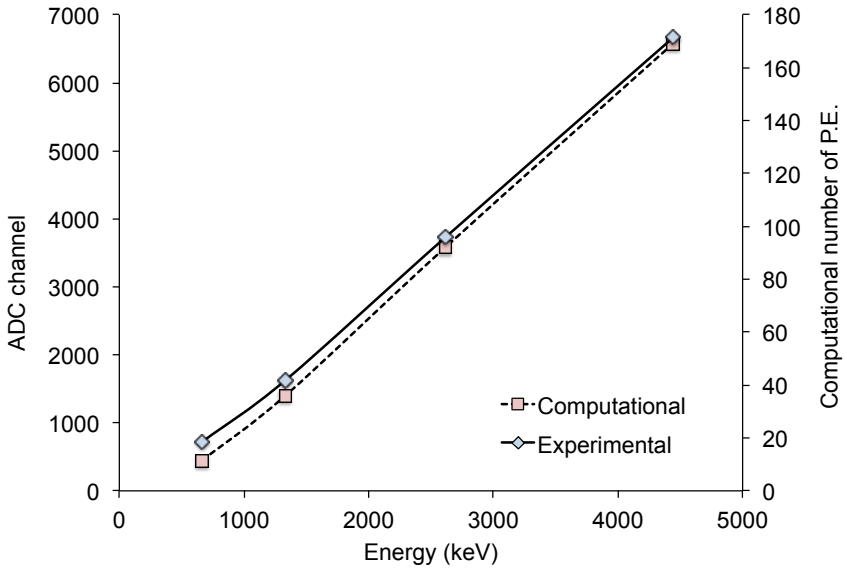

Figure 17: Correlation of simulation and experimental energy calibration for 2-inch long detector.

It is important to note that the relationship of incident photon energy versus Cherenkov photons produced exhibits a strong linear correlation in this energy range. However, slightly above the 4.4 MeV gamma ray energy this relationship breaks down. This is a combination of multiple factors, mostly PMT nonlinearity and the growing dominance of the pair production reactions inside the detector material. A lot of deposited energy is lost in the form of the two 511 keV photons from positron annihilation which don't significantly contribute to the Cherenkov generation as described in the Cherenkov energy threshold section. The linear relationship is only valid from 1 MeV to 4.4 MeV, if any other energies are to be considered a nonlinear relationship must be used.

The array of 8 quartz detectors was transported to MIT Bates Linear Accelerator Facility in Middleton, Ma for testing with the proposed nuclear reaction driven source. Once on site, the only sources available other than the accelerator were a ^{60}Co and a

PuBe source. Upon set up of the equipment, these sources we used to gather the two energy calibration points before any other experiments were performed. A spectrum of the raw beam was then collected for use in the energy calibration to apply to the rest of the experiments. This energy calibrated results can be seen in Figure 18.

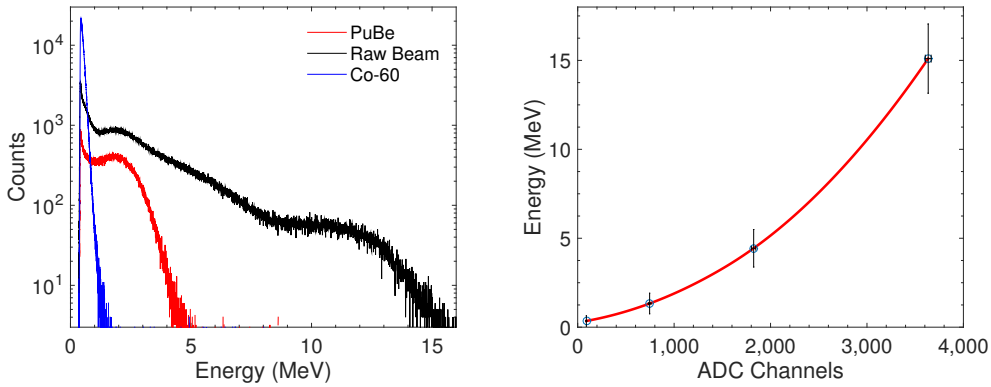

Figure 18: Calibrated spectral response of the 2-inch long detector (experimental).

The energy calibration relationship derived uses a second order polynomial fit shown in Equation 2 and reports the energy bin to energy conversion in keV. Only three sources were available at Bates for this calibration, ^{60}Co, PuBe, and the accelerator source. The calibration was augmented by including the PMT pedestal as the absolute Cherenkov energy threshold, 336 keV. The absolute threshold is the minimum energy needed to generate Cherenkov radiation and is therefore assumed to be related to a single photoelectron in the PMT. This forces a positive y-axis intercept while also giving an extra point for energy calibration.

$$Energy(bin) = 0.000985 * bin^2 + 0.472907 * bin + 343.530754 \quad (2)$$

The calibration was performed using fifteen digit precision in the polynomial fit. This many digits was not necessary for this detector because of the charge sensitivity of the digitizer was reduced, making the energy bins larger. The 15.1 MeV photons only needed about 3800 energy bins to span the entire spectrum. Reducing the sensitivity was necessary to ensure there were enough counts in each bin to be

significant. The level of precision is unnecessary, but since it is performed in a very efficient analysis code there is no need to reduce it.

The error bars shown in the right plot for Figure 18 is taken as the standard error of the energy and energy bin found by linear extrapolation described in the energy calibration section. The error in the y-direction, energy, is large due to the crude energy resolution available from Cherenov radiation. This error is thought to be overstated from repeated measurements of known energies, but is still included here until a more in-depth statistical analysis of the energy calibration method is available which is beyond the scope of this thesis.

CHAPTER IV

TRANSMISSION OF MONOENERGETIC PHOTONS THROUGH VARIOUS MATERIALS

4.1 Approach to analysis

Active interrogation systems must have highly penetrating radiation to be able to probe shielding in order to uncover illicit material. High energy photons from low energy nuclear reactions can penetrate such materials. Shielded special nuclear material presents a unique challenge due to the very high densities involved in the material itself as well as the shielding. The Beer-Lambert Law, Equation 3, is a simple way to calculate the transmission probability of known energy photons using atomic number related properties, mainly the energy-dependent mass attenuation coefficient μ/ρ and ξ, the areal density of the object.

$$T(E) = \frac{I(E)}{I_0(E)} = e^{(\frac{-\mu(E)}{\rho})*\xi} \tag{3}$$

The photon source considered in this thesis is the ^{11}B(d,n-γ)^{12}C producing high intensity 4.4 MeV and 15.1 MeV photons. The choice of this source takes advantage of the differences in Compton scatter and pair production cross sections over a range of materials. The 4.4 MeV photon interactions are dominated by Compton scattering reactions so analysis of the transmission of this photon is a direct measure of the density of the material it passes through. The 15.1 MeV photon interactions are dominated by pair production reactions for most materials as shown in Figure 19 adopted from Knoll [11] and modified.

The mass attenuation coefficients can be decoupled from the areal density in Equation 3 by taking a ratio of the transmission of the two energies and solving for the attenuation coefficients shown in Equation 4. This produces a figure of merit relating

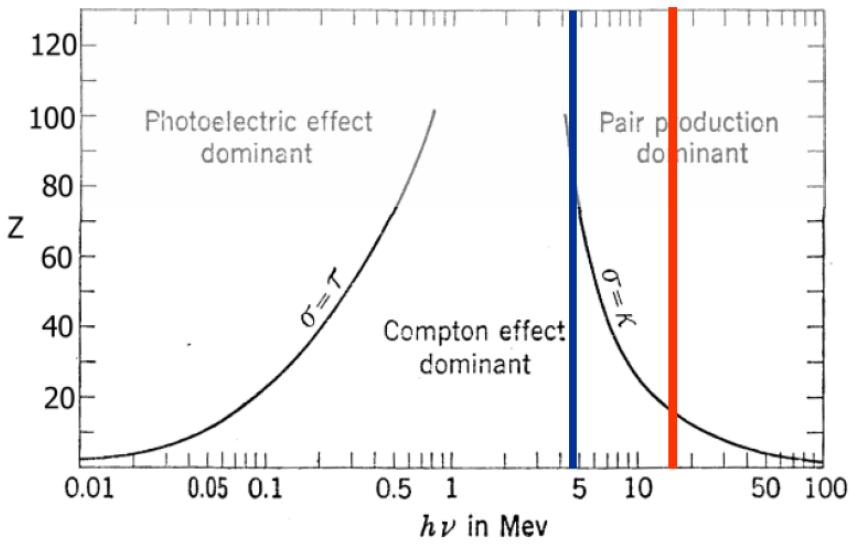

Figure 19: Relationship of gamma interaction probability as a function of energy and atomic number adopted from Knoll [11].

the energy dependent effective mass attenuation coefficients that is independent of the areal density, ξ.

$$\frac{ln(T(E_1))}{ln(T(E_2))} = \frac{\mu(E_1)}{\mu(E_2)} \tag{4}$$

The effective atomic number of an object composed of a mixture of elements can be defined by considering a hypothetical "pure" element with an areal density equal to that of a composite object where the pure elemental object produces the equivalent photon attenuation. Equation 3 can be rewritten for a composite object containing i independent materials as Equation 5. The measured ratios can be compared to a database of known attenuation coefficients to produce a Z_{eff} without needing any more information.

$$T = \Pi_i e^{-\frac{\mu}{\rho} * \xi_i} = e^{-\Sigma_i \frac{\mu_i}{\rho_i} * \xi_i} = e^{-(\frac{\mu}{\rho})_{eff} * \xi} \tag{5}$$

Once the Z_{eff} is determined. the areal density can easily be calculated from the transmission at either of the photon energies analyzed. Areal density may be desirable in some situations, but for the analysis presented here only the total transmission and Z_{eff} are of interest.

Figure 20 shows the total mass attenuation coefficients from NIST XCOM for selected materials spanning the material expected in cargo containers. A ratio of the 15.1 MeV to 4.4 MeV attenuation coefficients for many materials gives a series of figures of merit unique to the atomic number that can be compared to measured transmission values. This 15.1 MeV to 4.4 MeV ratio series can be used to quickly identify low-, mid-, and high-Z materials defined here as atomic number greater than about 65.

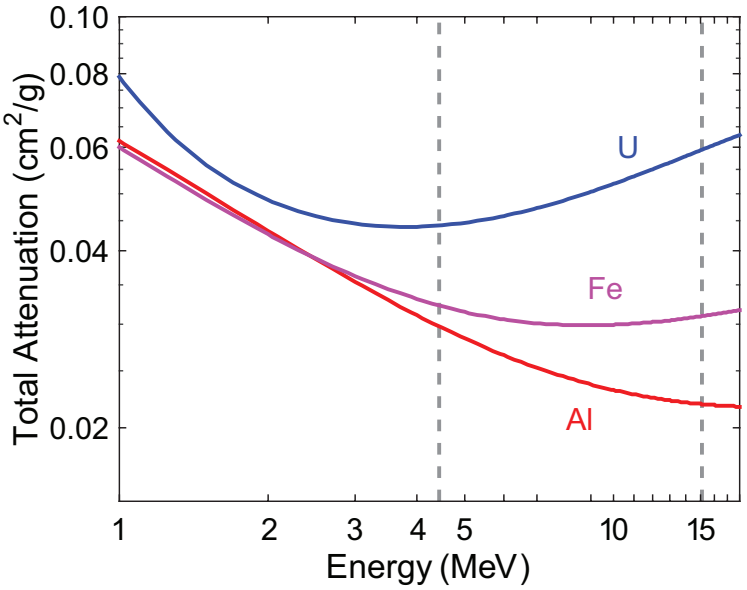

Figure 20: Total attenuation coefficient of select materials.

The analysis considered here assumes any photon interaction will remove that photon from the beam and hence is not considered transmitted. Although Compton Scattering at these energies is highly forward peaked, there is a large distance between the object of interest and the detectors making this a valid assumption.

4.2 Transmission in Geant4

Transmission simulations were performed early during the detector design phase to illuminate any extra consideration that may not have been evident. The studies were done using Geant4 and various detector design concepts.

The most complete transmission studies were conducted with a single Cherenkov detector, modeled as 1x1x12 inch block of acrylic, and 2x2x2 inch cube of representative materials between the planar gamma ray source and the detector. Materials studied include water, aluminum, lead, and natural uranium with a brief summary of the transmission results shown in Table 3. Air is artificially assigned a Z_{eff} for these studies due to the low density and the fact that it is the baseline for full transmission in lieu of vacuum.

Table 3: Summary of transmission results in the detector from Geant4 simulation for constant material size.

Material	Approximate Z_{eff}	4.4 MeV Transmission	15.1 MeV Transmission
Air	$\tilde{0}$	64%	45%
Water	7.2	55%	42%
Aluminum	13	58%	34%
Lead	82	35%	2%
Uranium	92	1%	0%

This data shows a very large difference in the gamma ray transmission as the approximate atomic number of the material increases. This table shows how many events occurred in the detector for each energy. The intrinsic efficiency of the detector, in air, is approximately 45% for the 15.1 MeV photons and 64% for the 4.4 MeV photons assuming 100% geometric efficiency. High efficiency, therefore long detectors, is crucial to minimize scanning time of the system. Note that the for high-Z materials, the difference between 4.4 MeV and 15.1 MeV gamma rays is very large, for example for lead, but tend to decrease for even higher Z materials, for example natural uranium. The difference is low for the uranium due to very efficient attenuation of all gamma rays. Thus, it is possible to not only search for high-Z materials, but potentially also distinguish SNM materials.

The integrated detection system will use algorithms incorporating ratio of the signals due to 4.4 MeV and 15.1 MeV and potentially other gamma rays to determine

the density of the material. Another form of information about the material is the shape of the response peak. Figure 21 graphically shows the detector responses to the transmission though various materials. The widths and heights of the peaks, as well as the ratios, yield a reliable understanding of the approximate Z of the material.

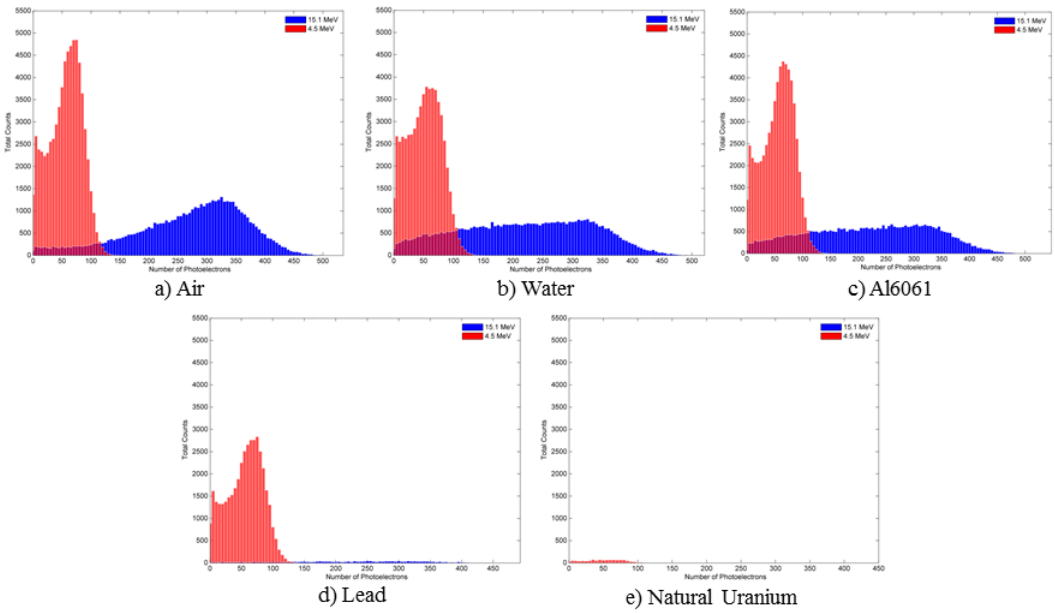

Figure 21: Transmission simulation results showing the response of both gamma ray energies per material. The 4.4 MeV response is in red and the 15.1 MeV response is in blue.

It is important to note these simulations represent a idealized scenario focused more on the transmission of photons rather than the detection. Many of the detector characteristics, such as optical photon propagation, are still included but were set to unrealistic efficiencies. This gives a good visual depiction of the concept. By integrating the correct peak areas and studying the peak shapes it is possible to glean information about the Z_{eff} of the material in question.

4.3 Experimental setup

Experimental studies of photon transmission was done at MIT Bates Linear Accelerator Facility in Middleton, MA using the modified DL-3 accelerator described earlier. An enriched ^{11}B target was not available at the time so a natural boron target was used. The target was surrounded by lead and borated poly sheets in all directions expect the direction of the detectors. This ensures a low dose rate to the surroundings as well as a reduction of scattering effects detected during measurements. The direction of the detectors is collimated using concrete blocks as well as lead and iron bricks as depicted in Figure 22.

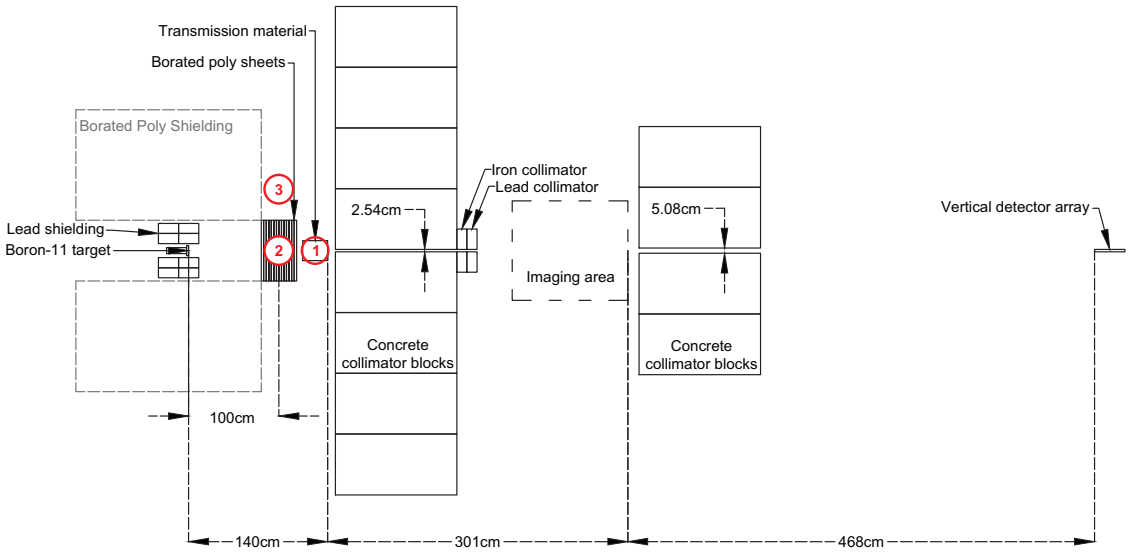

Figure 22: Diagram of the experimental set up showing the top view. This diagram is drawn to scale.

This configuration of shielding and collimation produces a fan beam from the isotropic de-excitation of the ^{12}C nucleus produced in the nuclear reaction. The beam divergence was calculated to be 8.62 mrad in the horizontal plane and 276 mrad in the vertical plane. The Cherenkov detector array was approximately 770 cm from the transmission targets. Transmission studies were carried out using approximately 36 cm of borated polyethylene immediately following the target as shown in Figure 23

to significantly reduce the neutron flux in the beam. The use of this borated polyethylene also reduced the low energy gamma rays produced in the reaction while having little effect on the 4.4 MeV and 15.1 MeV photons of interest. The quartz detectors are relatively immune to neutron reaction in the detectors themselves but the reduced neutrons lessens the probability of activation as well as neutron interactions in the transmission targets which may generate more gamma rays.

Figure 23: Photo of the target region (far left) to the detector array (far right).

This accelerator is currently housed in a warehouse that does not have shielded walls. The dose rates outside the warehouse must be kept below $0.5\,\mathrm{mrem\,h^{-1}}$ as dictated by the radiation safety officer on site. These requirements lead to a maximum operating beam current of about $20\,\mu\mathrm{A}$ instead of the expected $90\,\mu\mathrm{A}$ maximum of the system.

The Cherenkov detector mini-array consisting of 8 quartz detectors was placed a total of 909 cm from the natural boron target. The vertical center-line of the array was brought up to the vertical center-line of the beam by placing the array on an adjustable lift table and using a rotating laser level. This level was adjusted to project the axis of

Figure 24: Photo of the experimental set up starting from the deuterium plasma source at the bottom showing the linear accelerator, target, shielding, collimation, and then detectors from bottom to top respectively.

the RFQ accelerator all around the room. The horizontal center-line of the detector array was aligned with the horizontal beam center-line by matching a plum-bob from the center of the detectors to marks on the floor that were created by surveying when the accelerator was installed. As a quick check, a flood light was installed between the boron target and the first set of collimation and projected towards the detectors as shown in Figure 25.

The data acquisition system consisted of an 8-channel CAEN DT5730B digitizer running digital pulse processing pulse shape discrimination (DPP-PSD) firmware. The digitizer uses individual on-board field programmable gate arrays (FPGAs) to quickly digitize and analyze the pulses producing an energy bin count for each channel independently. After an event is processed on board it is sent to the control software on a laptop via USB where is it accrued in an energy bin versus count histogram. On board processing significantly reduces the data readout rate since only the channel number and integrated value of the event need to be transmitted instead of the entire

Figure 25: Flood light projected through collimation to show detector alignment with fan beamline.

waveform. This equipment contains on board memory to store events for processing if a second event occurs before the first one is processed. This leads to virtually zero deadtime due to electronics and processing to ensure integrity of very high count rates. The laptop also controls two CAEN DT5533N power supplies which are remotely controllable via CAEN software GECO2020 and the 65 foot active USB repeater cable. The laptop is housed in the control room with the operator for safety.

4.4 Experimental transmission results

The transmitted spectrum of multiple objects of varying Z was measured. These materials were placed between the borated poly and the first set of concrete collimators, depicted as position 1 in Figure 22. This placement ensured full coverage of the entire Cherenkov detector array for simultaneous measurements using all 8 detectors. The materials studied span a wide range of Z and thickness as reported in Table 4.

Table 4: Objects used for transmission studies with constant areal density. The atomic number of W corresponds to the Z_{eff} of the copper tungstate alloy.

Material	Z	Thickness (mm)	4.4 MeV Transmission	15.1 MeV Transmission
Al	13	71.05	59.7%	66.9%
Fe	26	24.62	57.2%	56.3%
Cu	29	21.40	54.5%	52.0%
Mo	42	19.54	52.8%	45.0%
Sn	50	26.56	53.3%	44.2%
W	69.5	8.81	58.7%	48.2%
Pb	82	19.29	41.5%	30.1%
U	92	10.16	41.3%	29.9%

After the beam was transmitted through these materials it was collimated by layers of concrete shielding blocks, lead, and iron bricks. All materials chosen for this experiment had approximately the same areal density of $19.5\,\mathrm{g\,cm^{-2}}$ except for the tungsten target. It was obvious from the measurements that this material did not fit the theory so the exact dimensions and mass of each material was collected. The density of each material was calculated from these measurements and then the areal density was recalculated. The tungsten sample was found to have a density of $16.7\,\mathrm{g\,cm^{-3}}$. Upon further investigation it was found this was not pure tungsten, but a copper tungstate allow generally referred to at Cu90W. This density and thickness presented an areal density of $14.6\,\mathrm{g\,cm^{-2}}$.

The opacity of these objects was measured for a time period of 2700 second using an average beam current of approximately 18 µA. The beam current varied slightly through out the experiments due to temperature effects on the RF high voltage supplies. The warehouse containing this accelerator is not temperature controlled so temperature fluctuations are expected. The measured spectra from select materials can be seen in Figure 26.

The left figure shows the measured transmitted spectra with integration regions for each energy shown in gray. These regions were integrated using a dynamic analysis

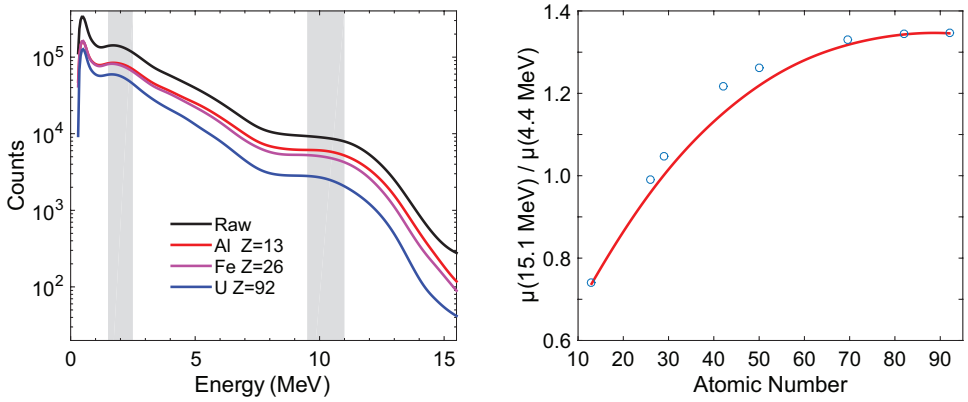

Figure 26: Detector response from select materials (left) including the areas of integration in gray used to calculate attenuation coefficients (right).

script created as part of this work for fast and consistent analysis of Cherenkov spectra. The script is optimized for speed to yield virtually instantaneous analysis of the spectra by calculating the integrals of both regions and calculating the 15.1 MeV to 4.4 MeV attenuation coefficient ratio presented in Equation 4. The right plot in Figure 26 shows these calculated ratios as circles and shows the theoretical ratios of the known materials as the fitted red curve. The experimental data is in close agreement with the expected curve for most of the Z range. The calculated error on the measured values was smaller than the size of the circled used to represent the points so they were neglected from the plot.

While the calculated ratios are a close match to the expected theoretical values, a more accurate method of interpolation between known points is needed. Instead of using the analytic curve, a relationship of the ratio to Z_{eff} can be determined by fitting the experimental data as shown in Figure 27.

This plot shows the ratios calculated from the 2 inch detector from the transmission experiment. This analysis was done for each detector individually to optimize results, but for consistency only one detector is used for illustration. The fitting analysis is broken up into two regions with an atomic number of Z=42, molybdenum, as the break point because a single quadratic does not fit the data well. A sum of

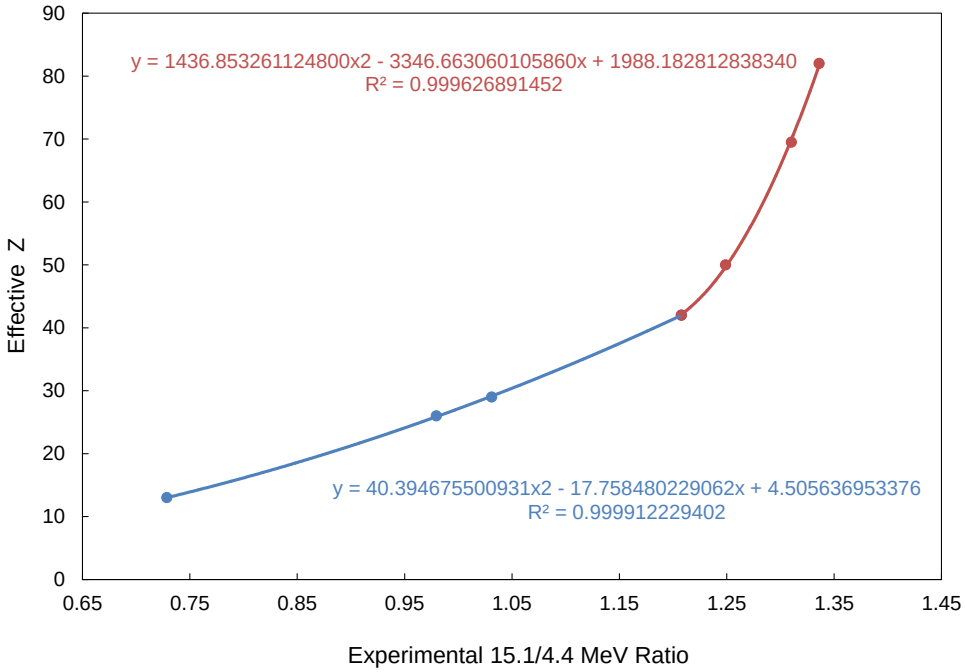

Figure 27: Experimental ratios from 2 inch detector with multi-region quadratic fitting.

exponentials fit was attempted but broke down quickly past the experimental range. The best fit was found to be two second order polynomials. These fitted relationships were inserted into the real-time analysis script with appropriate validity ranges for determination of unknown Z_{eff} from measured 15.1 MeV to 4.4 MeV attenuation coefficient ratios.

CHAPTER V

USE OF CHERENKOV DETECTORS IN ACTIVE INTERROGATION APPLICATIONS

Active interrogation applications pose great challenges for detector systems such as dead time, radiation damage, and pulse pileup. Cherenkov detectors are well suited to meet these challenges due to the physics of Cherenkov radiation as well as materials they can be made from. The speed of Cherenkov detectors is unrivaled when designed correctly. These detectors also offer a coverage area per cost that is not achievable by other detection techniques.

5.1 Deadtime in high flux environments

Studies were done to investigate dead time of the system to validate the use of these detectors in such a demanding environment. These studies were conducted with no borated polyethylene in the beam line to produce the maximum possible radiation flux. The absence of the borated polyethylene also means there is no longer a neutron filter to parse the neutrons from the beamline. The high energy neutrons can produce gamma rays through various reactions with materials all over the experimental hall adding to the demands on the detector systems. Figure 28 shows a summary of the results obtained from this experiment.

The beam current was varied starting at 8 µA and increased in 4 µA intervals. Each step was run for a total of 1800 s and the entire spectrum was integrated to give the total number of counts. This experiment was given special permission run operate the accelerator up to 24 µA by the radiation safety officer provided that access to the areas surrounding the building were restricted.

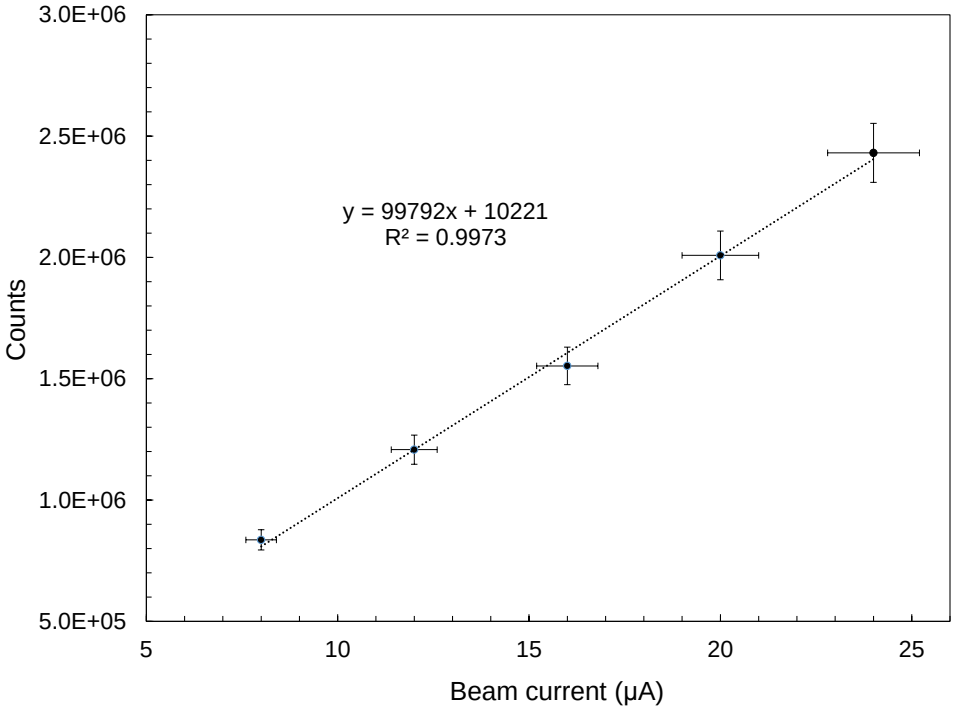

Figure 28: Experimental results from dead time studies showing resulting count rates from varying beam currents.

This study shows a very strong linear correlation between the accelerator beam current and the integral number of events in the detector. Over this range of beam currents there appears to be no indication of dead time in the detector system. It is incorrect to extrapolate this relationship beyond the experimental range, however it is promising that no dead time is observed. In the final application the beam current will be significantly higher but will include the neutron filter that was removed for this study. The final system will also have much more material, cargo containers, in the beam path reducing the radiation flux at the detector array.

5.2 Cost analysis and coverage of Cherenkov versus scintillators

Any detection system for active interrogation must balance cost, scalability, and necessary energy resolution to achieve desired performance. It has already been shown that energy resolution is not a priority when using a source such as the one employed here. Some of the main concerns for this application are cost, scalability, and image spatial resolution. High spatial resolution requires a large amount of small detectors packed closely together. It has been suggested many times to use NaI detectors for these types of application due to the relatively low cost as compared to other scintillators. NaI detectors are available from Saint-Gobain measuring $5.08 \times 10.16 \times 40.64$ cm for this type of application. However, these detectors are on the order of $8,000 each and the smallest face is 5.08×10.16 cm which dictates the smallest pixel size possible in an imaging application. These detectors are highly sensitive to natural background as well as low energy activation products which add huge demands to an active interrogation system. The Cherekov detectors designed here cost about $50 each not including the PMT and are only 2.5 cm in diameter which means the number of possible pixels is increased by a factor of about 8 over the NaI detectors. If the cylindrical Cherenkov detectors are offset vertically, as they are designed here, the pixel density per area is a factor of 10 higher for the Cherenkov system than it is for the NaI system. PMTs can be purchased in bulk for the Cherekov detectors for $324 each or SiPMs can be applied for as little as $84 per detector.

Scintillators also have to rely on decay times which can fluctuate heavily depending on temperature as shown in Figure 29. Temperature effects are very important as a system such as this needs to be able to operate consistently and reliably under exposure to the weather conditions. It is not possible to operate in a climate controlled environment at all times therefore temperature effects must be considered.

Operation of an active interrogation system in cold temperatures is a very real

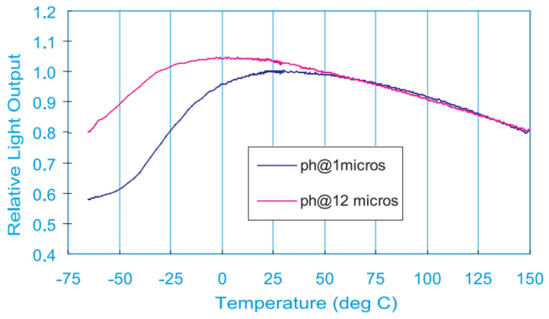

Figure 2. Temperature response of NaI(Tl)

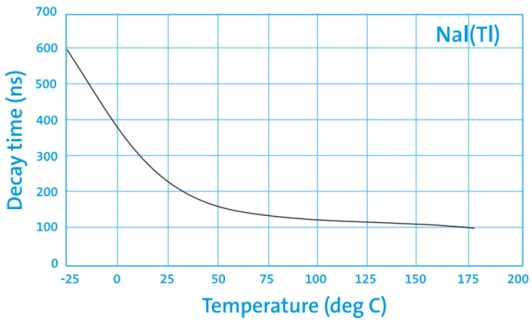

Figure 3. Temperature dependence of the decay time of NaI(Tl)

Figure 29: NaI decay and light output as a function of temperature.

possibility. Figure 29 shows the light output (left) and decay time (right) as a function of temperature for NaI crystals. Temperatures around freezing, 0 °C, are very common but pose a large problem for NaI detectors as the decay time nearly doubles with respect to room temperature and the light output per incident energy significantly decreases. As the temperature changes through out the day, this detector will have to be constantly re-calibrated and the analysis of the signal must change as well. The increased decay time will lead to more pulse pileup and dead time that must be accounted for. The quartz Cherenkov detectors are immune to these temperature effects as well as neutron interactions making them a much more stable, reliable, and simple alternative to the NaI detectors.

5.3 Dose measured from monoenergetic source

Dose from active interrogation systems is a concern not only for the cargo, but also for potential stowaways. Non interrogated areas can be shielded to protect the operators and bystanders, but the interrogated material will have exposure. The use of highly penetrating monoenergetic photons significantly reduces the dose delivered to the cargo as opposed to bremsstrahlung beams.

The dose rate delivered to the interrogated material was measured in the beam line. These measurements were conducted under the same shielding conditions as the

transmission experiments, i.e. with 14 inches of borated polyethylene in place. The gamma dose was measured by an ion chamber manufactured by Fluke Biomedical, Inovision model 451P. The neutron dose measurement was made with a NRD 9 inch neutron ball containing a ^{10}B proportional counter and manufactured by Thermo Scientific Corporation as show in Figure 30.

Figure 30: Dose measured in beamline in the cargo area between collimators.

These meters have been recently calibrated as they are the survey instruments used by the radiation safety officer on site. Both dose meters were operated in integration mode and run separately for 5 minutes each in the beam line. Background measurements were taken immediately after accelerator operation to account for any potential activation products in the experimental set up. The resulting dose from gamma rays was calculated to be $(0.360 \pm 0.016)\,\mathrm{mrem\,h^{-1}\,\mu A^{-1}}$ and the dose resulting from neutrons not filtered out by the borated polyethylene was calculated to be

$(0.104 \pm 0.005)\,\mathrm{mrem\,h^{-1}\,\mu A^{-1}}$. These number are calculated on a $\mathrm{h^{-1}\,\mu A^{-1}}$ basis to be scaled to any operating configuration as the scanning time is inversely proportional to the beam current

CHAPTER VI

CONCLUSIONS AND FUTURE WORK

Detection of shielded special nuclear material is an arduous task that poses unique challenges, especially while in transit. The focus of this research aims to resolve some of those issues with a novel detector design and application as an imaging system as well as analysis techniques. This work has shown that Cherenkov detectors with proper design considerations can be useful in active interrogation systems. These detectors have the ability to operate in intense background situations, such as near accelerators, with little to no effect on the detection system. Most any sort of active interrogation system uses an accelerator as the radiation source so the intense low energy background is always present.

The purpose of this thesis was to investigate the principles design, spectral analysis, and applicability of Cherenkov detectors for active interrogation applications. The work focused on monoenergetic gamma ray active interrogation sources and detection system in the search for SSNM. The following objectives were fulfilled by the research conducted for this thesis:

- Design and optimization of Cherenkov detectors for use with low energy nuclear reaction sources
- Create a method of spectral analysis from Cherenkov detectors
- Relate the transmission of monoenergetic photons to the Z_{eff} of the interrogated material
- Construct and study the proof of concept system in realistic scenarios

6.1 Summary of work completed

6.1.1 Computational model for detector design and optimization

The computational model described in Chapter 3 was developed as a design and optimization tool for the design of Cherenkov detectors. This Geant4 model includes all electromagnetic and optical photon processes involved in Cherenkov radiation as applied to detectors. The model is capable of inducing and tracking optical processes, including the generation of Cherenkov photons by a charged particle, transition radiation, and transport of associated particles. The model incorporates detector geometry, optical photon absorption coefficients, optical boundary properties, reflector properties, and PMT quantum efficiencies for various PMTs considered.

The resulting Cherenkov detector design was constructed and experimentally validated in the laboratory. The design employs high purity quartz, SiO_2, as the Cherenkov radiator medium for its relatively high density and superior optical photon transmission capabilities, especially in the UV region. This material is also virtually immune to neutron reactions in the energy range produced by the low energy nuclear reaction source.

6.1.2 Energy calibration of Cherenkov detectors

Cherenkov detectors suffer from poor energy resolution due to the continuous nature of the physics taking place including energy transfer from a photon to a charged particle by means of Compton scattering and pair production. Further compounding this issue is the bremsstrahlung losses of the high energy electrons and the charged particle slowing down to the region of the characteristic low energy threshold for Cherenkov radiation production. Cherenkov spectroscopy is generally not possible or even attempted for most applications.

Use of the quasi-monoenergetic source helps to mitigate the need for high energy

resolution due to the well separated gamma energies available. A new energy calibration method was developed as part of this work based on physics related artifacts in the acquired spectra. By using pronounced inflection points and slopes in the spectra we are able to assign a charge collected versus known incident energy relationship to generate a reliable energy calibration. This spectral information is crucial to apply the proposed method of analysis to uncover illicit SNM.

6.1.3 Transmission analysis to unfold Z_{eff}

A method to calculate the Z_{eff} of the interrogated material was devised by considering the transmission of multiple gamma ray energies through that material. The 1-D analytic Beer-Lambert law was used to back calculate the energy dependent mass attenuation coefficient for the traversed material using multiple gamma ray energy responses in the detector. Then, the areal density of the material was decoupled by using ratios of the mass attenuation coefficients of certain energies leaving a ratio of only the energy dependent attenuation coefficients.

This methodology was applied to many materials commonly found in cargo containers and some that should not be there, such as depleted uranium. The ratios were build for all materials tested and compare well with the analytic prediction. The experimental values were then fit using a multi-region technique based on the dominance of the physics interactions to produce a relationship of attenuation coefficient ratios to the atomic number. Composite materials interrogated are then compared to the experimental and analytic relationships and are assigned a Z_{eff} based on the attenuation coefficient ratio.

6.2 Resulting publications and presentations

The work in this thesis has resulted in publications as proceeding and peer reviewed journals as well as presentations at conferences and seminars.

6.2.1 Accepted publications and presentations

- 2014: Proceedings: INMM 55^{th} Annual Meeting. "Detection of Shielded Special Nuclear Material Using High Energy Gamma Ray Transmission Imaging and Cherenkov Detectors". **Awarded best student paper in division.**

- 2014: Presentation: INMM 55^{th} Annual Meeting. "Detection of SSNM Using High Energy Gamma Ray Transmission Imaging and Cherenkov Detectors".

- 2015: Peer Reviewed Journal: Nuclear Instruments and Methods A: P.B. Rose Jr., A.S. Erickson, Calibration of Cherenkov detectors for monoenergetic photon imaging in active interrogation applications, Nucl. Instrum. Meth. A, Vol. 799, no. 1, pp. 99-104 (2015).

- 2015: Presentation: The 2015 International Conference on Applications of Nuclear Techniques Crete, Greece "Cherenkov Detector Imaging System for Active Interrogation

- 2015: Presentation: Georgia Tech NRE-MP Seminar Series. "Low-Dose Inspection for Nuclear Threats Using Monochromatic Gamma-Rays

- 2015: Presentation: American Physical Society - Division of Nuclear Physics. "Low-Dose Inspection for Nuclear Threats Using Monochromatic Gamma-Ray Transmission Imaging

6.2.2 Peer reviewed publications currently under review/submission

- Scientific Reports: "Uncovering Special Nuclear Materials by Low-energy Nuclear Reaction Imaging"

- Applied Physics Letters: "Monochromatic Imaging of Special Nuclear Materials with Cherenkov Detectors"

6.2.3 Awards received based on the work presented in this thesis

- INMM: Best student paper in division
- Achievement Rewards for College Scientists (ARCS)

6.3 Future work

This project is currently being extended to imaging studies using the detectors, energy calibration, and Z unfolding algorithms presented in this thesis. This will include high contrast planar images of the overall transmission as well as a pixel by pixel evaluation using the attenuation coefficient ratio method to produce a map of the Z_{eff}. This will include single materials and composites to include uranium material. I am also extending the ratio analysis to include multiple energy integration areas to produce other ratio relationships to refine the analysis method. This is meant to produce a real-time analysis of the interrogated material.

The project is also being extended into new detectors using SiPMs to fine spatial resolution which will require more advanced modeling and simulation as the system becomes more complex. The imaging system will also be integrated with a novel composite neutron detectors under development by collaborators at Pennsylvania State University to monitor for delayed neutrons. This integration will give us multiple methods to detect SSNM for a more complete proof of concept system. This system will then be operated under many types of active interrogation sources such as Inverse Compton, bremsstrahlung, and other low energy nuclear reaction driven sources.

REFERENCES

[1] Agostinelli, S., "Geant4–a simulation toolkit," *Nucl. Instrum. Meth. A*, vol. 506, pp. 250–303, 2003.

[2] Allison, J. and others, "Geant4 developments and applications," in *IEEE Trans. Nucl. Sci.*, vol. 53, pp. 270–278, 2006.

[3] Antolak, A. J., Doyle, B. L., Leung, K. N., and others, "Active interrogation using low-energy nuclear reactions," in *SPIE: Penetrating Radiation Systems and Applications VII*, vol. 5923, pp. 1–9, 2005.

[4] Brandis, M., Dangendorf, V., Piel, C., and others, "Nuclear reaction based radiation source for explosives and snm detection in massive cargo," in *AIP Conference Proceedings*, vol. 1336, pp. 711–716, 2005.

[5] Cherenkov, P., "Vidimoe svechenie chistykh zhidkostei pod deistviem γ-radiatsii," *Dokl. Akad. Nauk SSSR*, vol. 2, p. 451, 1934.

[6] Cherenkov, P., "Visible radiation produced by electrons moving in a medium with velocities exceeding that of light," *Phys. Rev*, vol. 52, pp. 378–379, 1937.

[7] Chichester, D. L. and Seabury, E. H., "Active neutron interrogation to detect shielded fissionable material," in *International Topical Meeting on Nuclear Research Applications and Utilization of Accelerators*, vol. SM/EN-02, 2009.

[8] Hamm, R., "Test report - factory acceptance tests," Tech. Rep. PO C1877, 2005.

[9] Jones, J., Blackburn, B., Watson, S., and others, "High-energy photon interrogation for non proliferation applications," *Nucl. Instrum. Meth. B*, vol. 261, pp. 326–330, 2007.

[10] Jones, J., Norman, D., Haskell, K., and others, "Detection of shielded nuclear material in a cargo container," *Nucl. Instrum. Meth. A*, vol. 562, pp. 1085–1088, 2006.

[11] Knoll, G. F., *Radiation detection and measurement*. Wiley, 3 ed., 21010.

[12] Kurennoy, S., Garnett, R., and Rybarcyk, L., "Intense combined source of neutrons and photons for interrogation based on compact deuteron rf accelerator," in *23rd Conference on Application of Accelerators in Research and Industry, CAARI 2014*, 2014.

[13] Lanza, R. C., Erickson, A., Fisher, J., and others, "Nuclear reaction based monoenergetic gamma ray radiography system for detection of nuclear materials," in *Nuclear Science Symposium and Medical Imaging Conference (NSS/MIC)*, 2014.

[14] Ludewigt, B., Antolak, A., Henestroza, E., and others, "Coaxial mono-energetic gamma generator for active interrogation," in *AIP Conference Proceedings: CAARI2008*, 2008.

[15] Rose Jr., P. B. and Erickson, A., "Detection of shielded special nuclear material using high energy gamma ray transmission imaging and cherenkov detectors," in *INMM Annual Meeting*, 2014.

[16] Rose Jr, P. and Erickson, A., "Calibration of cherenkov detectors for monoenergetic photon imaging in active interrogation applications," *Nucl. Instrum. Meth. A*, vol. 799, pp. 99–104, 2015.

[17] Runkle, R. C., Chichester, D. L., and Thompson, S. J., "Rattling nucleons: New developments in active interrogation of special nuclear material," *Nucl. Instrum. Meth. A*, vol. 663, pp. 75–95, 2012.

[18] Schubert, W., "On the security of our seaports." statement before the Committee on the Judiciary Subcommittee on Technology, Terrorism, and Government Information United States Senate, February 26 2002.

[19] Sowerby, B., "Cerenkov detectors for low-energy gamma rays," *Nucl. Instrum. Meth.*, vol. 97, pp. 145–149, 1971.

[20] Taddeucci, T. and Sheffield, R., "Neutron and gamma-ray production with low-energy beams," Tech. Rep. LA-UR-07-2724, Los Alamos National Laboratory, 2007.

[21] Ziock, K., Craig, W., Fabris, L., and others, "Large area imaging detector for long-range, passive detection of fissile material," *IEEE Trans. Nucl. Sci.*, vol. 51, pp. 2238–2244, 2004.